Atomically dispersed Fe–TM pairs on g-C_6N_6: A comparative theoretical insight into heteronuclear dual-atom catalysts for N_2 reduction to ammonia and urea

*Anjumun Rasool [a], Romana Khanam [a], Kubra Masood [a], and Manzoor Ahmad Dar [a]**

[a] Department of Chemistry, Islamic University of Science and Technology,

Awantipora, Jammu and Kashmir-192122, India

Table of contents

10. **Fig. S8.** Simulated free-energy pathways for direct urea formation from N_2 and CO_2 along Consecutive mechanism on Fe-Y and Fe-Ti respectively with potential determining step represented by red colour.
11. **Fig. S9.** Optimized truncated side views of NRR intermediates of different intermediates involved in the direct coupling of N_2 and CO_2 to urea on the (a) Fe-Ti and (b) Fe-Y HDACs. Red and blue coloured arrows indicate enzymatic and consecutive mechanisms respectively.
12. **Fig. S10.** Optimized truncated side views of NRR into ammonia intermediates on (a) Fe-V and (b) Fe-Cr HDACs along alternating and distal mechanisms. Purple and green coloured arrows indicate alternating and distal mechanisms respectively.
13. **Fig. S11.** Optimized truncated side views of NRR into ammonia intermediates on Fe-Mn HDACs along enzymatic and consecutive mechanisms. Red and blue coloured arrows indicate enzymatic and consecutive mechanisms respectively.
14. **Fig. S12.** Optimized truncated side views of NRR into ammonia intermediates on (a) Fe-Mo, (b) Fe-Rh and (c) Fe-Ru HDACs along alternating and distal mechanisms. Purple and green coloured arrows indicate alternating and distal mechanisms respectively
15. **Fig. S13.** Optimized truncated side views of NRR into ammonia intermediates on (a) Fe-La, (b) Fe-Ta and (c) Fe-Ir HDACs along alternating and distal mechanisms. Purple and green coloured arrows indicate alternating and distal mechanisms respectively
16. **Table S3.** Comparison of computed limiting potential of present studied best NRR into ammonia catalysts with the already studied systems
17. **Table S4**. Comparison of computed limiting potential of present studied best HDACs catalysts for urea formation via C-N coupling with the reported catalysts
18. **Table S5**: Free energy change of PDS on most promising Fe-TM candidates in consideration of the Hubbard U correction
19. **Fig. S14.** The projected density of states (PDOS) of (a) 3d, (b) 4d, and (c)5d transition metal-based Fe-TM HDACs. The PDOS of the total, TM-d, Fe-d, N-2p, and C-2p is plotted in grey, yellow, blue and green colours, respectively.
20. **Fig. S15.** PDOS, Charge difference density, and COHP of absorbed N_2 on the screened (a) 4d and 5d based Fe-TM systems. The contour level is set to 0.001 e/Å^3. The net Bader charge accumulated on the adsorbed N_2 is depicted using red arrow in the charge density difference plots.
21. **Fig. S16.** (a) The relationship between the adsorption energy of the most favorable $*N_2$ configuration and the Bader charge (Q_b). (b) Linear relation between the adsorption energy of

the most favorable $*N_2$ configuration and total d-states of the transition metal atoms near Fermi level (-1.0 to 1.0 eV).

22. **Fig. S17.** Fluctuations of temperature and energy during ab-initio Molecular Dynamics (AIMD) simulations of the best catalysts i.e. (a)Fe-V, (b)Fe-Ti, (c)Fe-Y and (d)Fe-Ir at 300 K for 20 ps
23. **Fig. S18.** Electronic band structure of (a) g-C_6N_6 monolayer (b) Fe-V, (c)Fe-Ti, (d)Fe-Y and (e)Fe-Ir
24. **Table S6.** Energy, ZPE, TS, G and ΔG of reaction steps of NRR into urea via direct N_2 and CO_2 coupling on Fe-Ti and Fe-Y along enzymatic and consecutive mechanisms
25. **Table S7.** Energy, ZPE, TS, G and ΔG of reaction steps of NRR into ammonia on Fe-V, and Fe-Cr along alternating and distal mechanisms
26. **Table S8.** Energy, ZPE, TS, G and ΔG of reaction steps of NRR into ammonia on Fe-Mn enzymatic and consecutive mechanisms
27. **Table S9.** Energy, ZPE, TS, G and ΔG of reaction steps of NRR into ammonia on Fe-Mo, Fe-Ru and Fe-Rh along alternating and distal mechanisms
28. **Table S10.** Energy, ZPE, TS, G and ΔG of reaction steps of NRR into ammonia on Fe-La, Fe-Ta and Fe-Ir along alternating and distal mechanisms

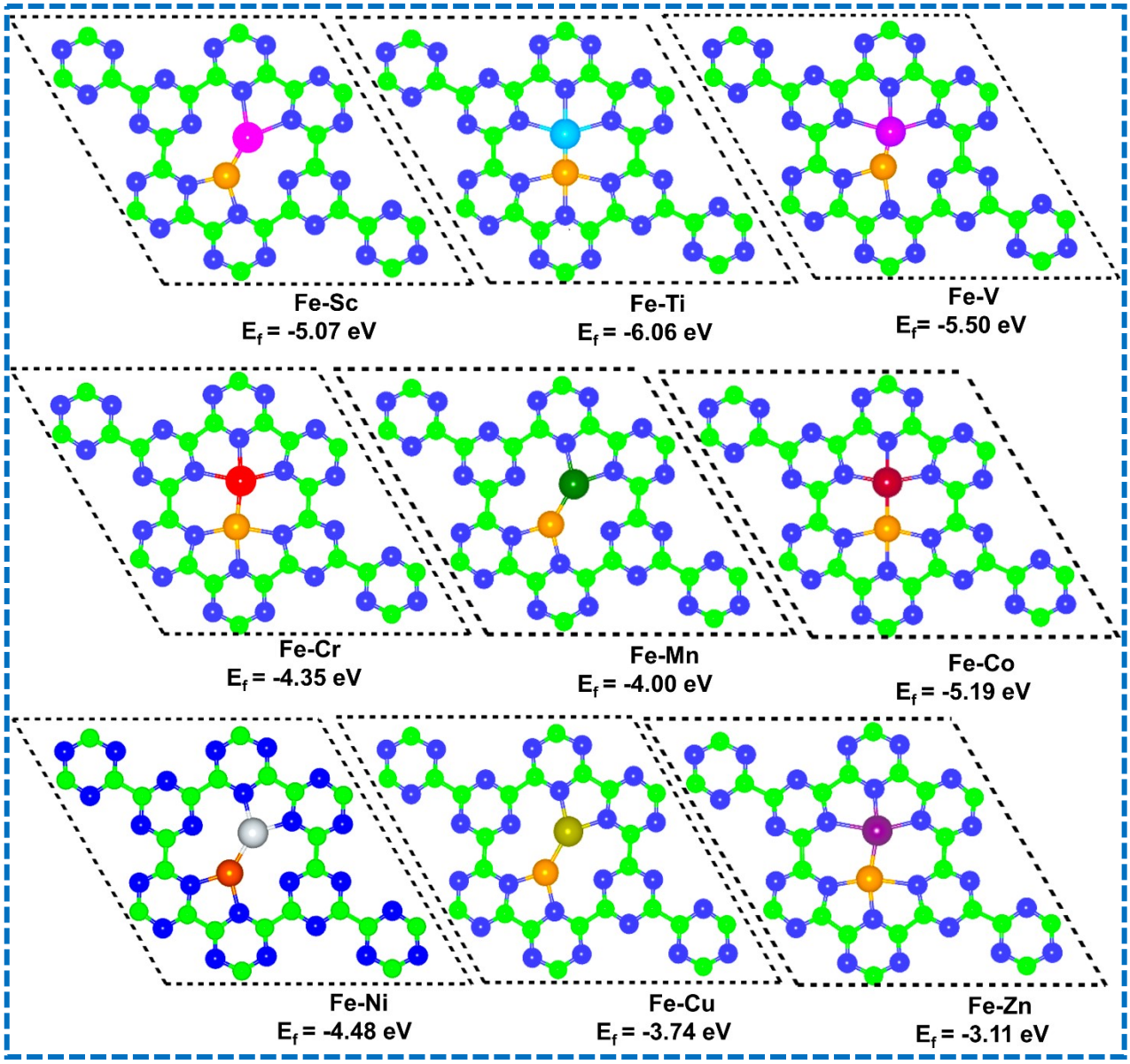
Fe-Sc
E_f = -5.07 eV
Fe-Ti
E_f = -6.06 eV
Fe-V
E_f= -5.50 eV
Fe-Cr
E_f = -4.35 eV
Fe-Mn
E_f = -4.00 eV
Fe-Co
E_f = -5.19 eV
Fe-Ni
E_f = -4.48 eV
Fe-Cu
E_f = -3.74 eV
Fe-Zn
E_f = -3.11 eV

(a)

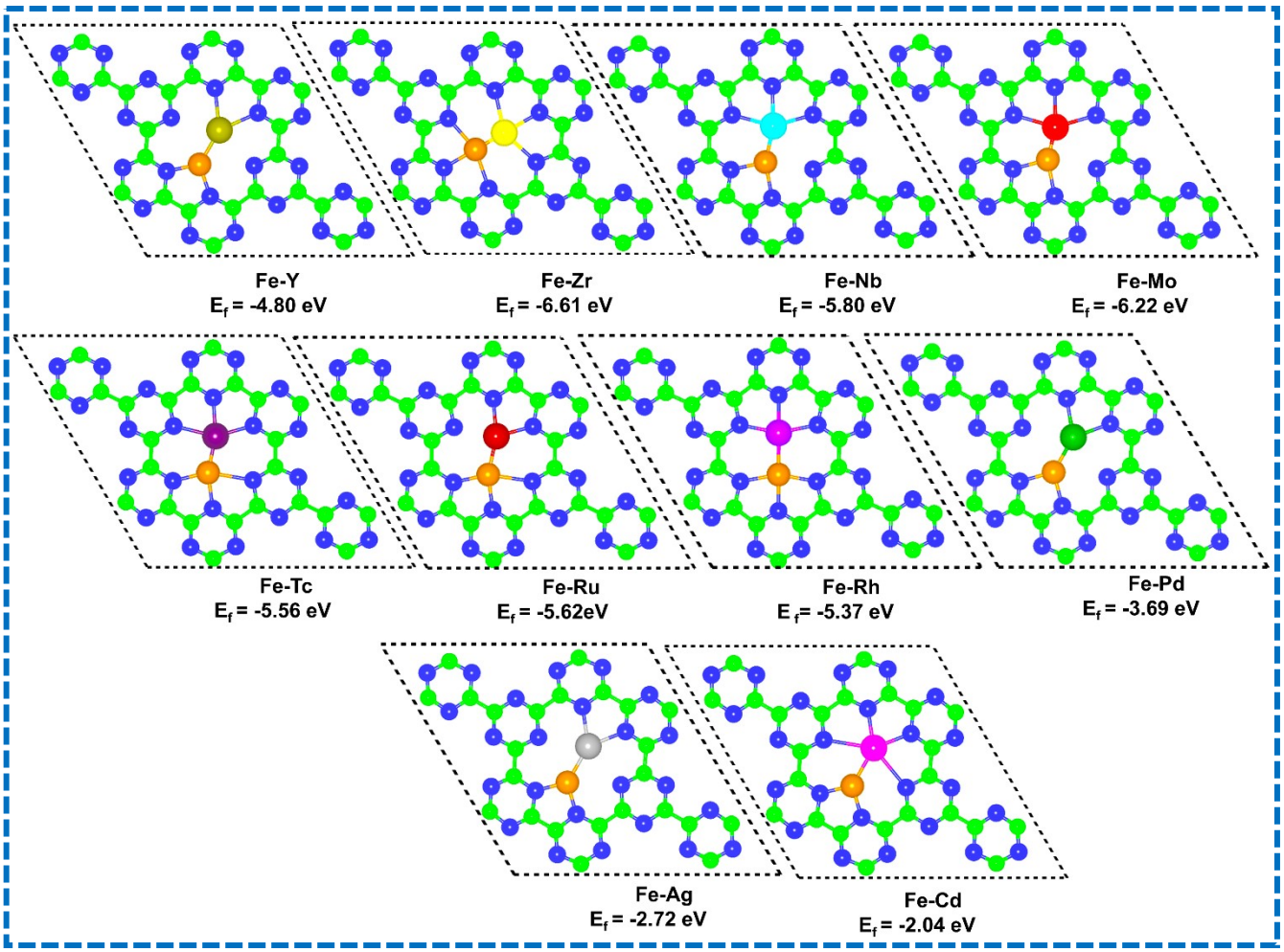
Fe-Y
E_f = -4.80 eV
Fe-Zr
E_f = -6.61 eV
Fe-Nb
E_f = -5.80 eV
Fe-Mo
E_f = -6.22 eV
Fe-Tc
E_f = -5.56 eV
Fe-Ru
E_f = -5.62eV
Fe-Rh
E_f = -5.37 eV
Fe-Pd
E_f = -3.69 eV
Fe-Ag
E_f = -2.72 eV
Fe-Cd
E_f = -2.04 eV

(b)

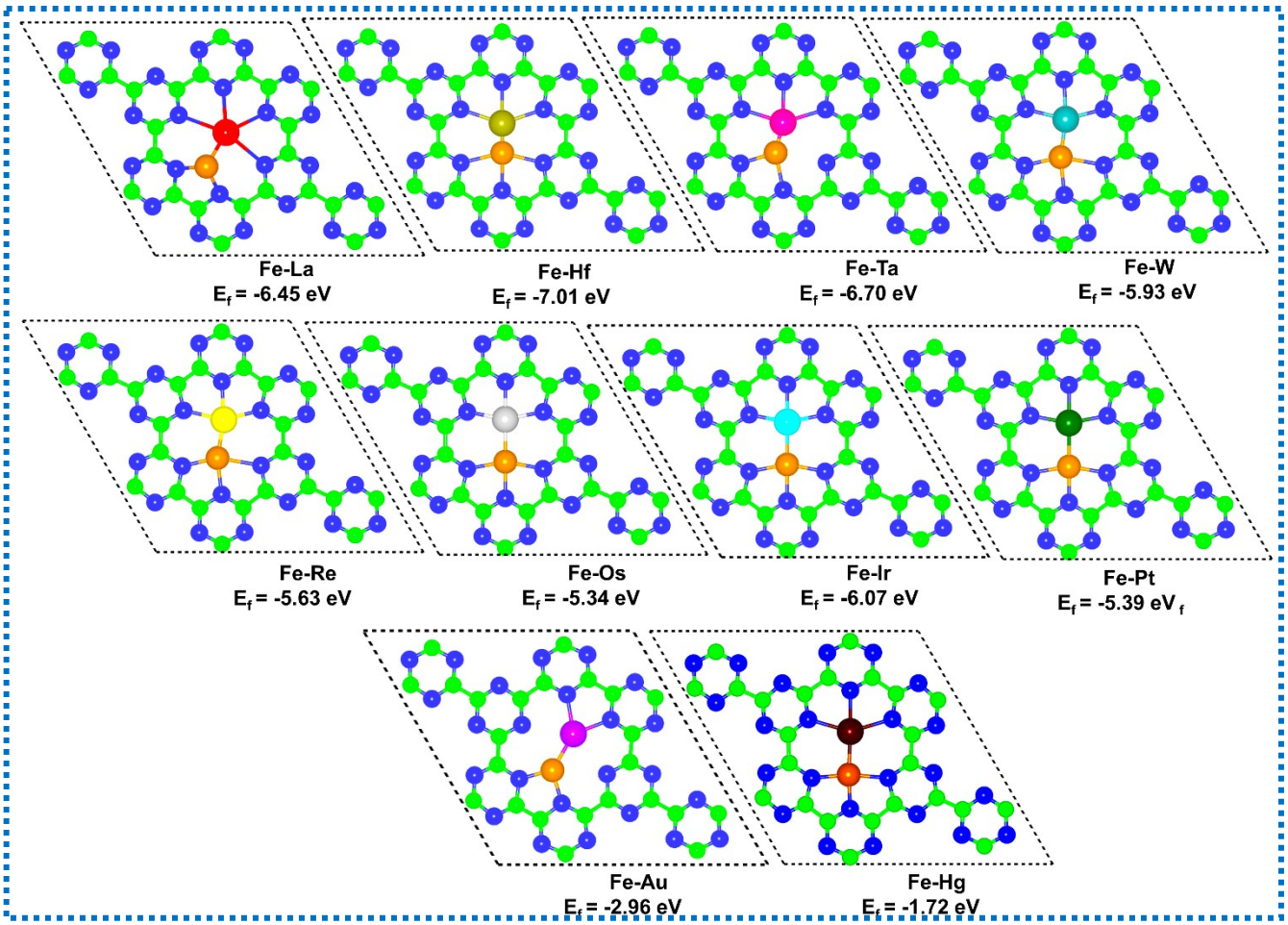

(c)

Fig. S1. Top views of the optimised geometries of (a) 3d, (b) 4d, and (c) 5d transition metal-based Fe-TM HDACs anchored on g-C_6N_6 monolayer with formation energy pervalues.

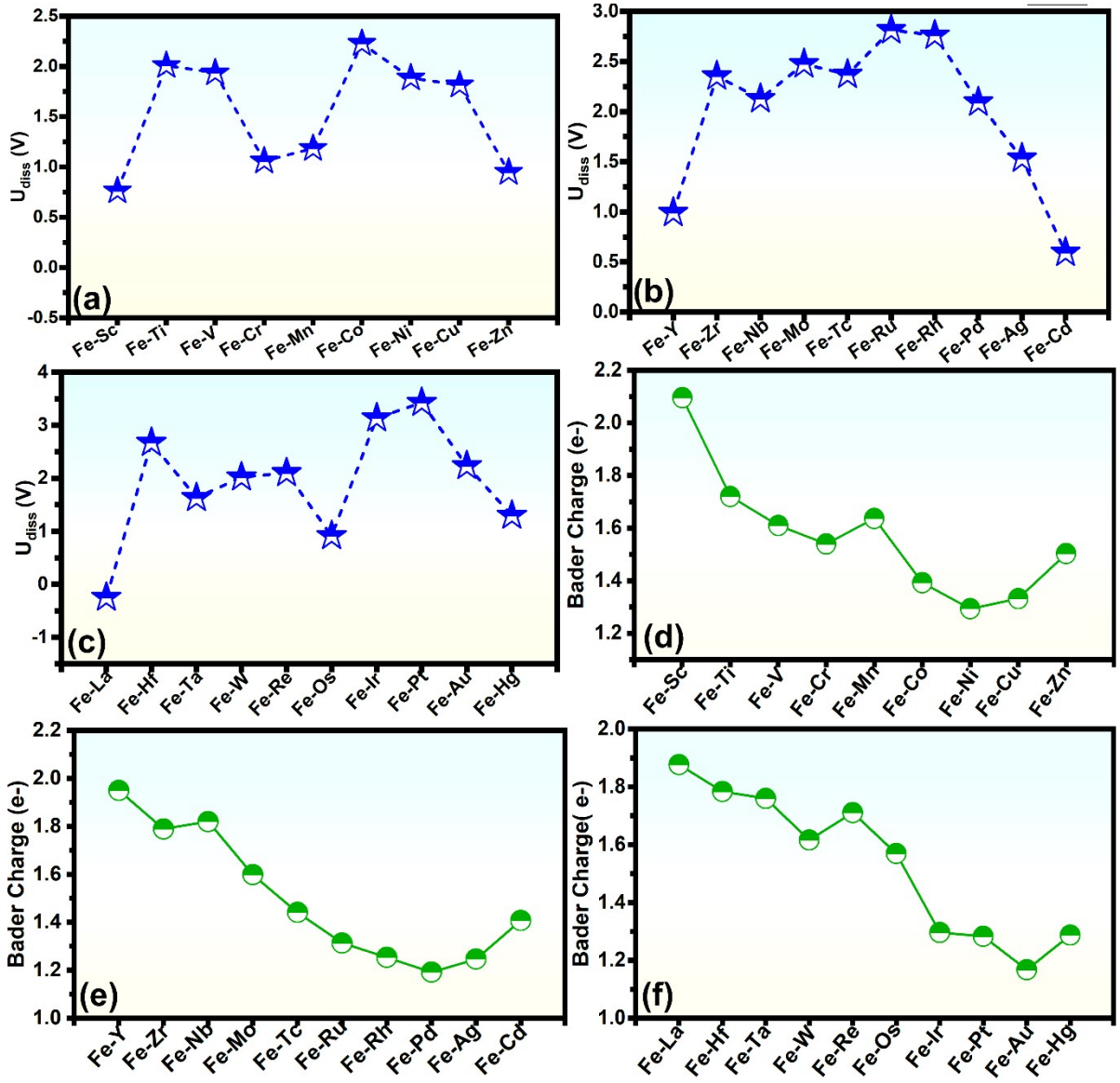

Fig. S2. Computed dissolution potential (U_{diss}) of (a)3d, (b) 4d and (c) 5d transition metal-based Fe-TM HDACs supported on the g-C_6N_6 monolayer. Bader charge ($Q_{Fe\text{-}TM}$) on the (d)3d, (e) 4d and (f) 5d transition metal-based Fe-TM HDACs supported on the g-C_6N_6 monolayer.

Table S1. The dissolution potential of Fe-TM HDACs. U^o_{diss} and N_e are the standard dissolution potential of bulk metal and the number of transferred electrons involved in the dissolution, respectively.

System	U^o_{diss}	E_f	N_e	U_{diss}
Fe-Sc	-1.26	-5.07	2.50	0.76
Fe-Ti	-1.03	-6.08	2.00	2.01
Fe-V	-0.82	-5.50	2.00	1.94
Fe-Cr	-0.68	-4.34	2.50	1.06
Fe-Mn	-0.82	-5.03	2.00	1.18
Fe-Co	-0.37	-5.19	2.00	2.23
Fe-Ni	-0.36	-4.48	2.00	1.89

Fe-Cu	-0.06	-3.74	2.00	1.82
Fe-Zn	-0.61	-3.11	2.00	0.95
Fe-Y	-1.41	-4.80	2.50	0.99
Fe-Zr	-0.95	-6.61	3.00	2.35
Fe-Nb	-0.78	-5.80	2.50	2.13
Fe-Mo	-0.64	-6.22	2.00	2.47
Fe-Tc	-0.41	-5.56	2.50	2.37
Fe-Ru	0.01	-5.62	2.00	2.81
Fe-Rh	0.08	-5.37	2.00	2.76
Fe-Pd	0.25	-3.69	2.00	2.09
Fe-Ag	0.18	-2.72	1.50	1.53
Fe-Cd	-0.43	-2.04	2.00	0.59
Fe-La	-2.83	-6.45	2.50	-0.25
Fe-Hf	-2.00	-7.01	1.50	2.67
Fe-Ta	-1.05	-6.70	2.50	1.63
Fe-W	-0.35	-5.93	2.50	2.02
Fe-Re	-0.15	-5.63	2.50	2.10
Fe-Os	-0.15	-5.32	5.00	0.91
Fe-Ir	0.71	-6.07	2.50	3.14
Fe-Pt	0.73	-5.39	2.00	3.43
Fe-Au	1.05	-2.96	2.50	2.23
Fe-Hg	0.46	-1.72	2.00	1.30

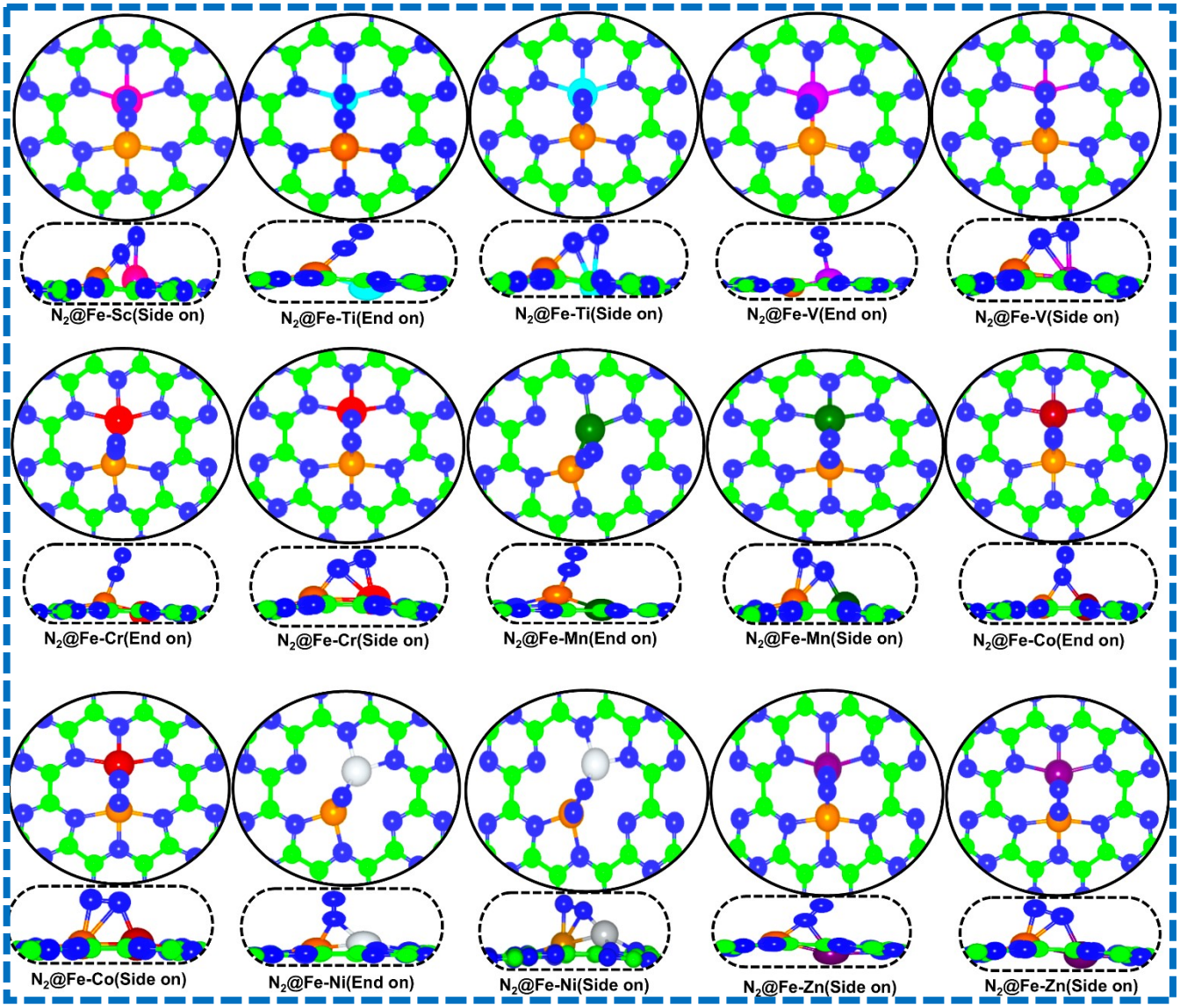
N2@Fe-Sc(Side on)
N2@Fe-Ti(End on)
N2@Fe-Ti(Side on)
N2@Fe-V(End on)
N2@Fe-V(Side on)
N2@Fe-Cr(End on)
N2@Fe-Cr(Side on)
N2@Fe-Mn(End on)
N2@Fe-Mn(Side on)
N2@Fe-Co(End on)
N2@Fe-Co(Side on)
N2@Fe-Ni(End on)
N2@Fe-Ni(Side on)
N2@Fe-Zn(Side on)
N2@Fe-Zn(Side on)

(a)

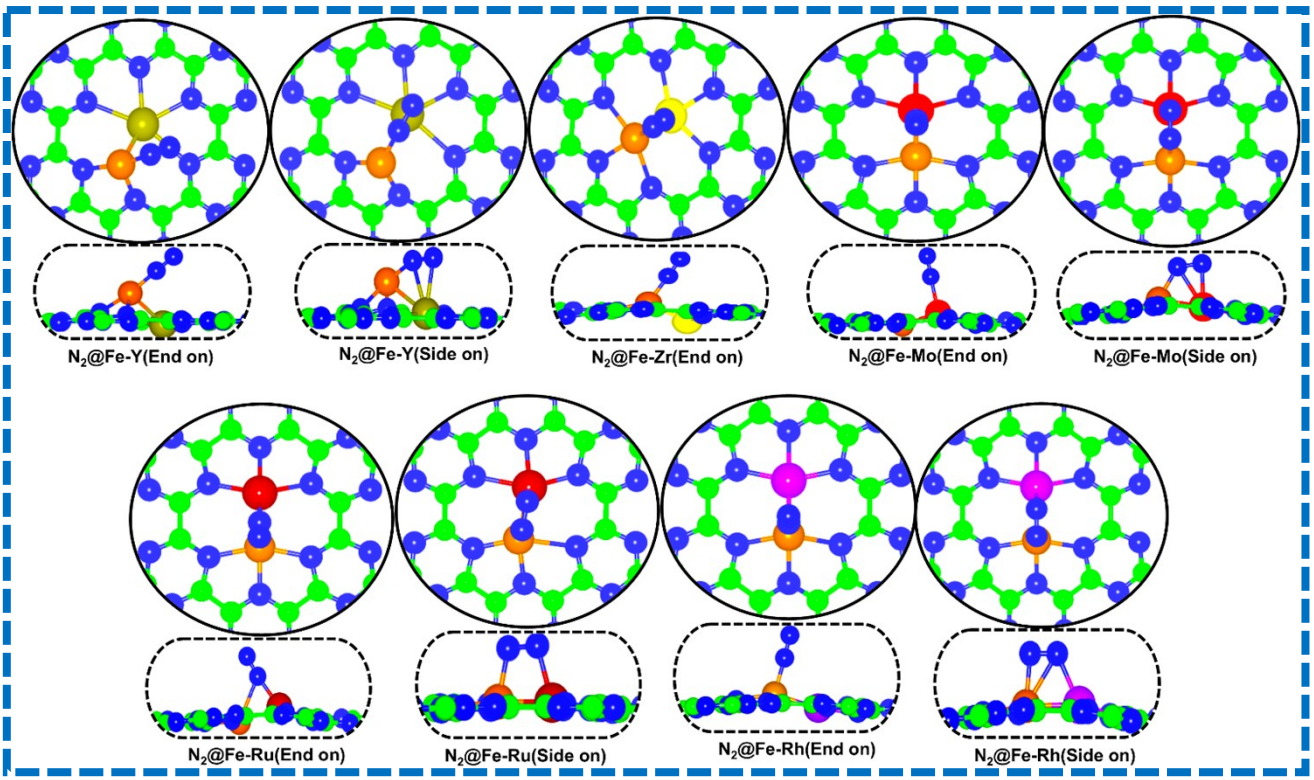

(b)

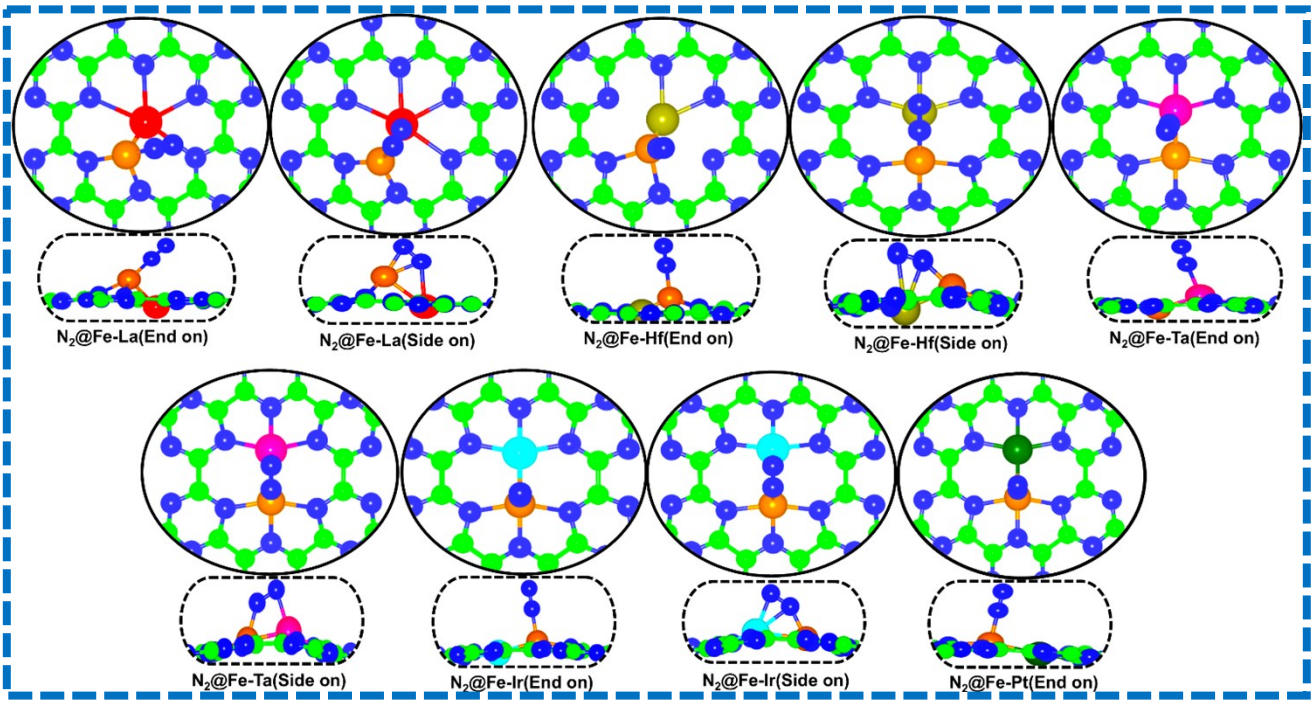

(c)

Fig. S3. Optimized truncated top and side views of N_2 chemisorbed structures on (a) 3d, (b) 4d, and (c) 5d Fe-TM HDACs

Table S2. Calculated N_2 binding energy (E_{ads}) in eV, N≡N (R_{N-N}) bond length in **Å**, and net Bader charge (Q_b) on the N_2 molecule adsorbed on Fe-TM HDACs

System	E_{ads} (eV)	R_{N-N} (Å)	Q_b (e) on N_2
Fe-Sc	-2.80	1.15	-0.63
Fe-Ti	-1.21	1.17	-0.60
Fe-V	-1.09	1.13	-0.26
Fe-Cr	-1.59	1.14	-0.34
Fe-Mn	-1.97	1.19	-0.61
Fe-Co	-0.88	1.15	-0.39
Fe-Ni	-1.19	1.18	-0.56
Fe-Zn	-1.29	1.15	-0.49
Fe-Y	-3.62	1.18	-4.86
Fe-Zr	-1.17	1.14	-0.54
Fe-Mo	-1.52	1.14	-0.30
Fe-Ru	-1.25	1.14	-0.35
Fe-Rh	-0.81	1.13	-0.26
Fe-La	-1.70	1.14	-0.39
Fe-Hf	-0.77	1.13	-0.23
Fe-Ta	-1.65	1.14	-0.33
Fe-Ir	-0.83	1.14	-0.54
Fe-Pt	-0.52	1.13	-0.21

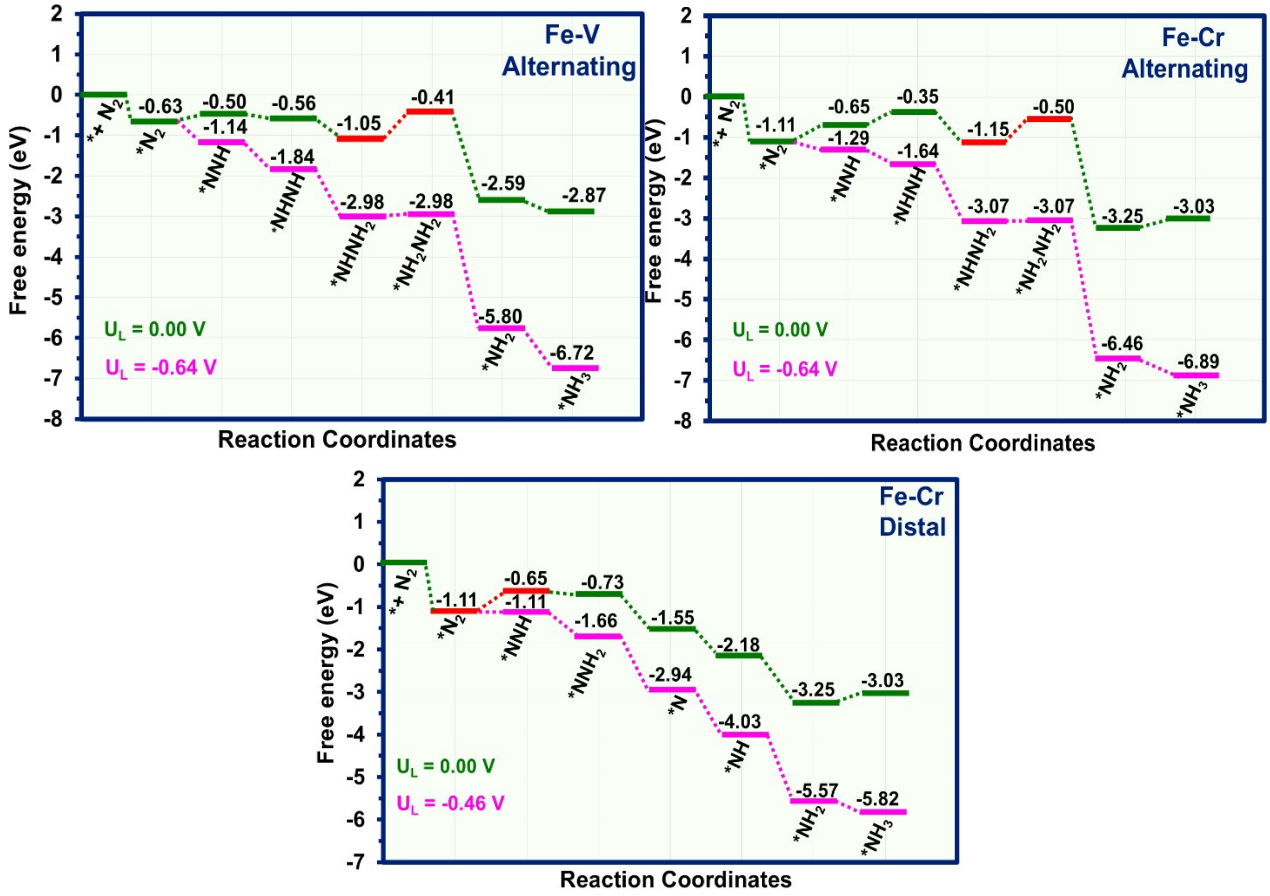

Fig. S4. Computed free energy profile for NRR into ammonia on Fe-V along alternating mechanism and on Fe-Cr along alternating and distal mechanisms with potential determining step represented by red colour.

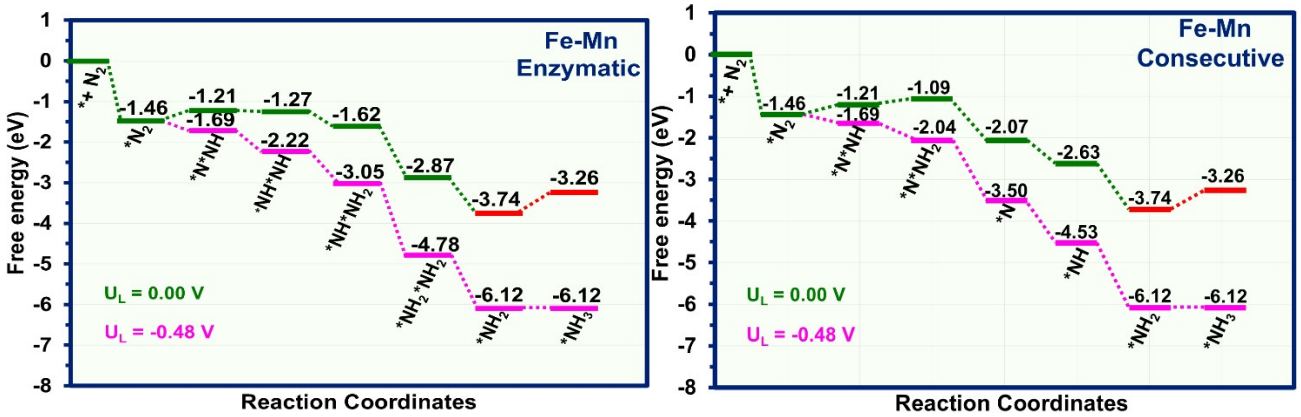

Fig. S5. Computed free energy profile for NRR into ammonia on Fe-Mn along Enzymatic and Consecutive mechanisms with potential determining step represented by red colour.

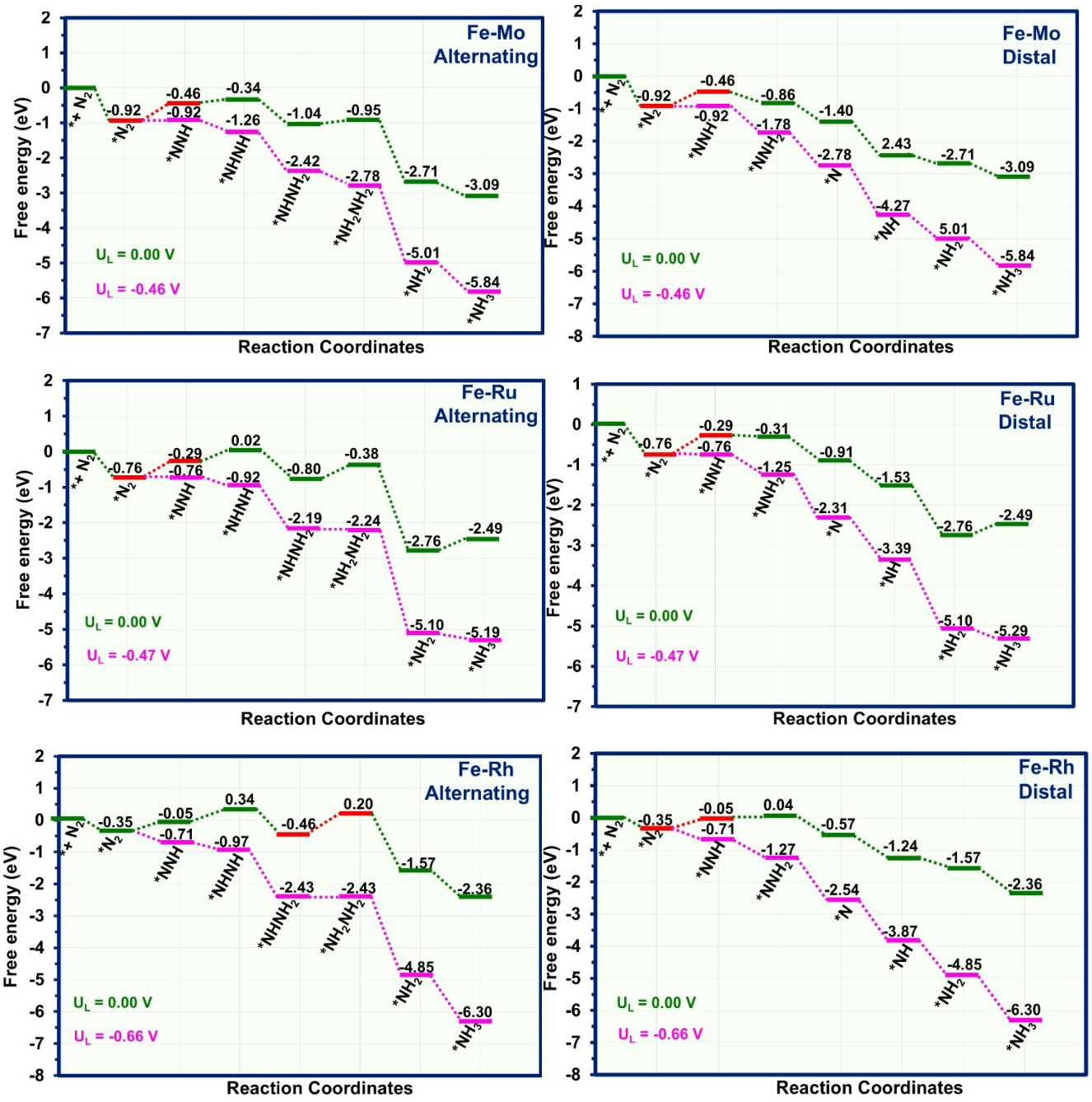

Fig. S6. Computed free energy profile for NRR into ammonia on Fe-Mo, Fe-Ru and Fe-Rh along alternating and distal mechanisms with potential determining step represented by red colour.

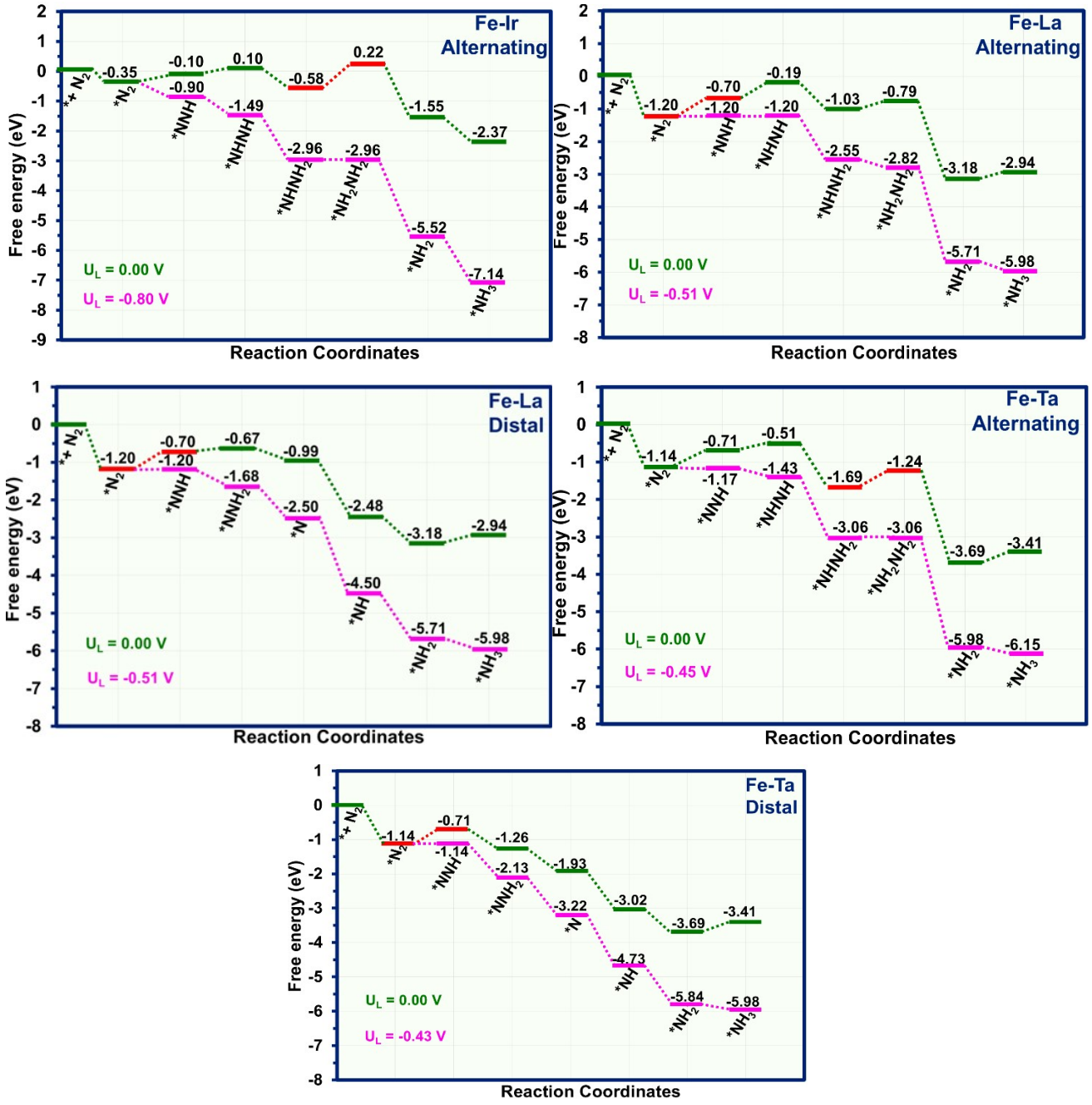

Fig. S7. Computed free energy profile for NRR into ammonia on Fe-Ir along alternating mechanism and on Fe-La and Fe-Ta along alternating and distal mechanisms with potential determining step represented by red colour

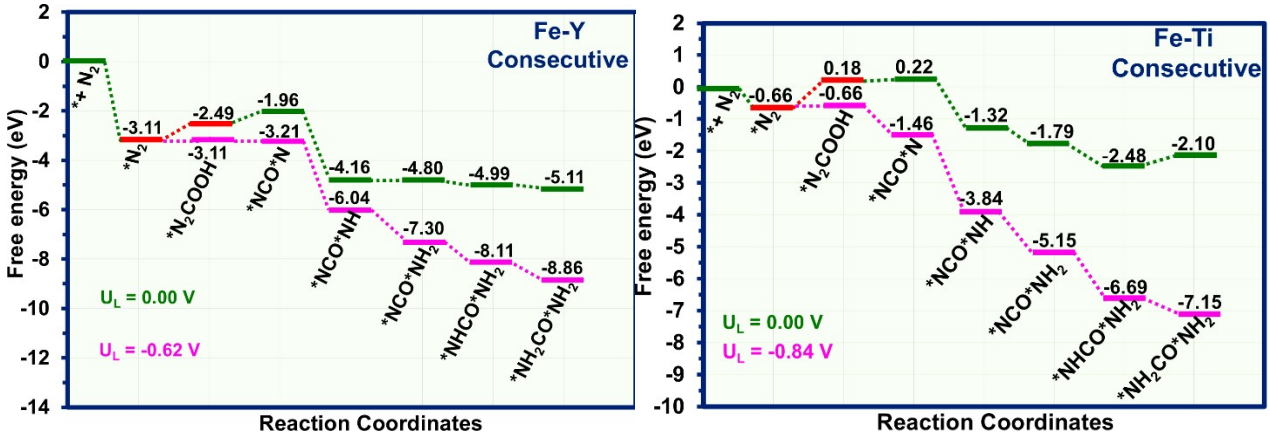

Fig. S8. Simulated free-energy pathways for NRR into urea along Consecutive mechanism on Fe-Y and Fe-Ti respectively with potential determining step represented by red colour.

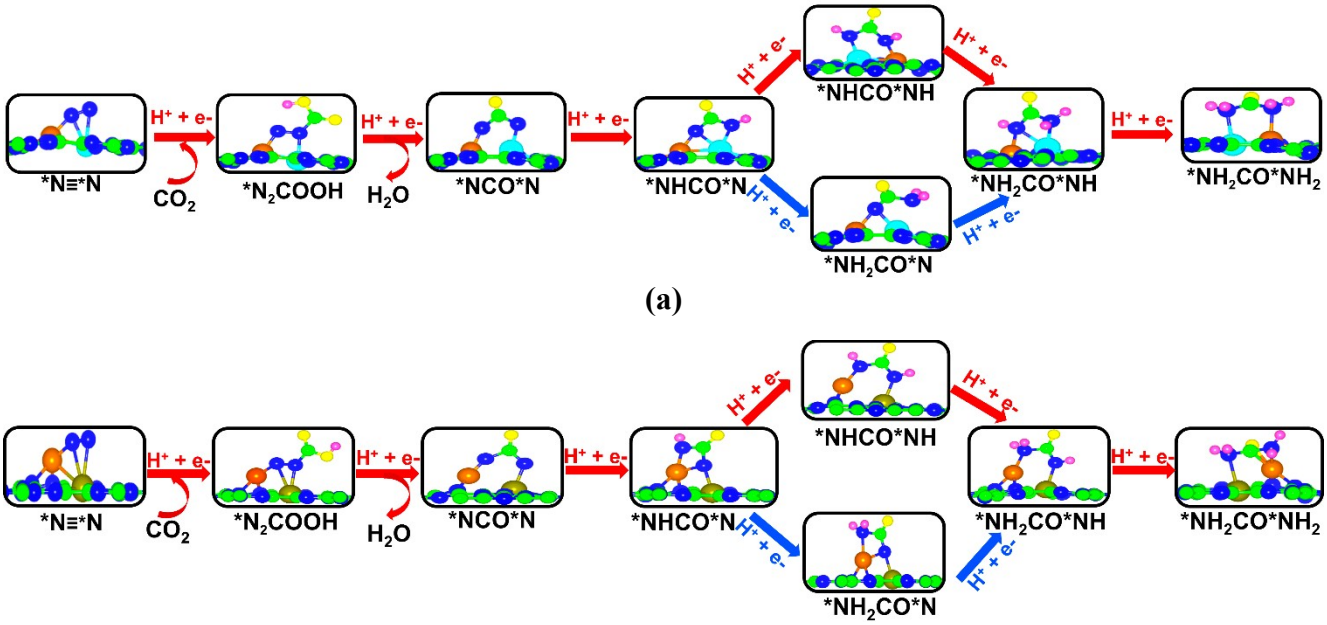

(a)

(b)

Fig. S9. Optimized truncated side views of NRR into ammonia intermediates of different intermediates involved in the NRR into urea on the (a) Fe-Ti and (b) Fe-Y HDACs. Red and blue coloured arrows indicate enzymatic and consecutive mechanisms respectively.

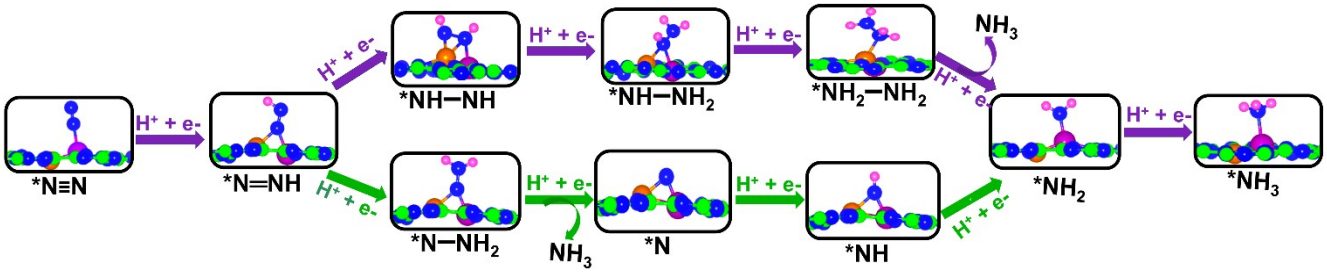

(a)

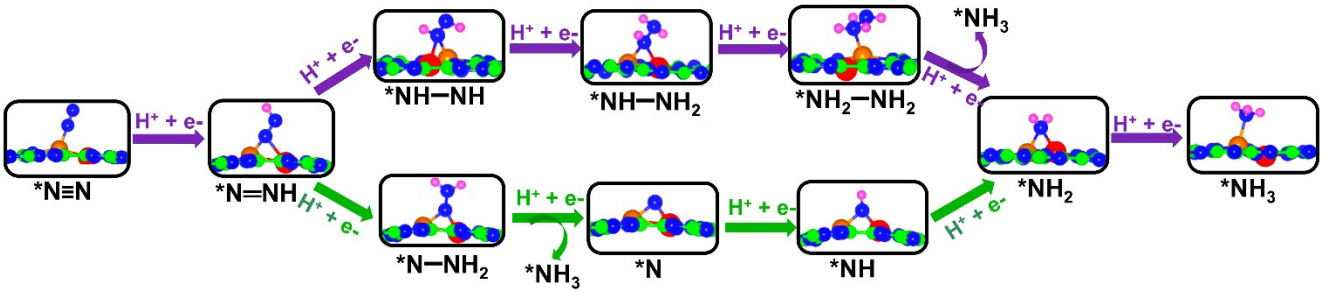

(b)

Fig. S10. Optimized truncated side views of NRR into ammonia intermediates on (a) Fe-V and (b) Fe-Cr HDACs along alternating and distal mechanisms. Purple and green coloured arrows indicate alternating and distal mechanisms respectively.

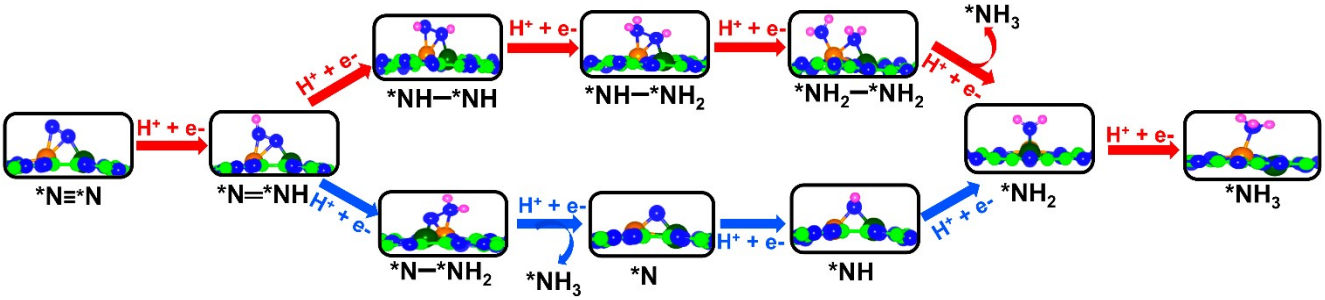

Fig. S11. Optimized truncated side views of NRR into ammonia intermediates on Fe-Mn HDACs along enzymatic and consecutive mechanisms. Red and blue coloured arrows indicate enzymatic and consecutive mechanisms respectively.

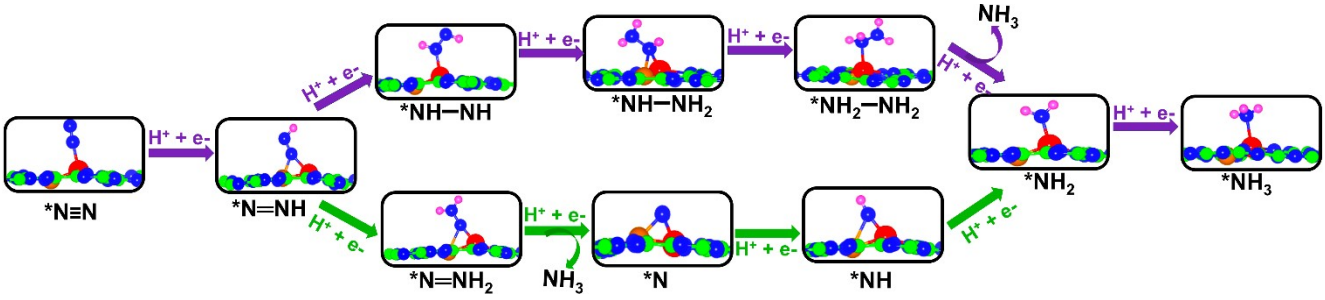

(a)

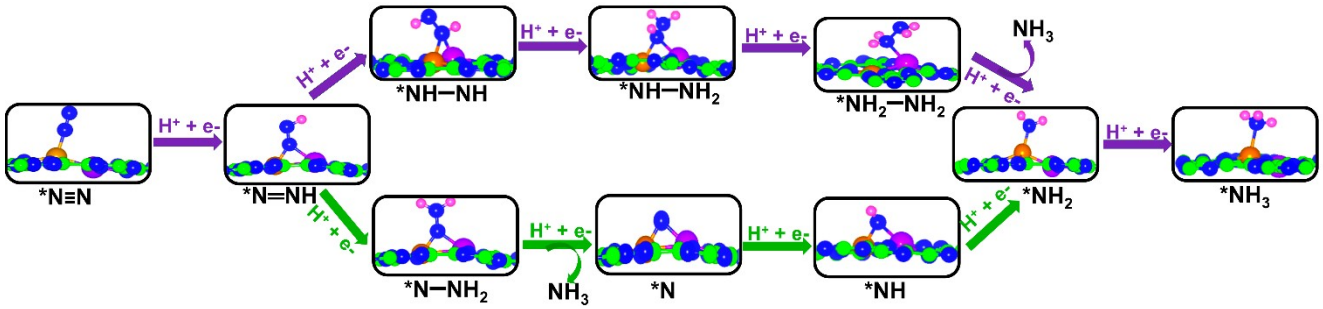

(b)

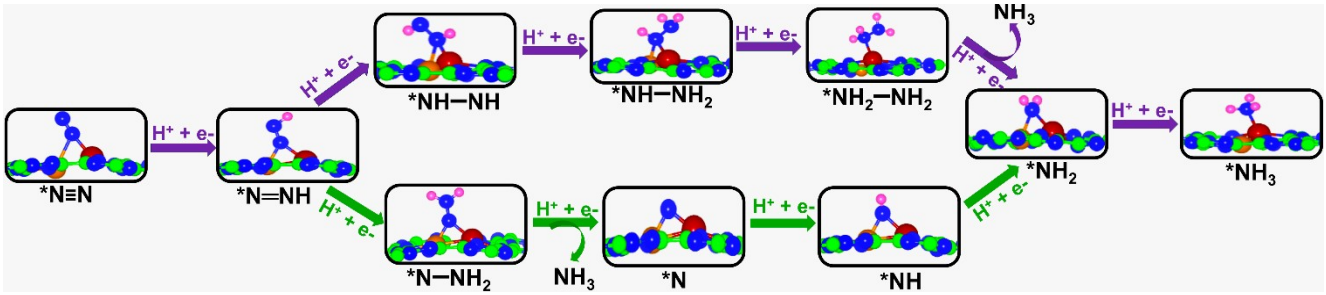

(c)

Fig. S12. Optimized truncated side views of NRR into ammonia intermediates on (a) Fe-Mo, (b) Fe-Rh and (c) Fe-Ru HDACs along alternating and distal mechanisms. Purple and green coloured arrows indicate alternating and distal mechanisms respectively.

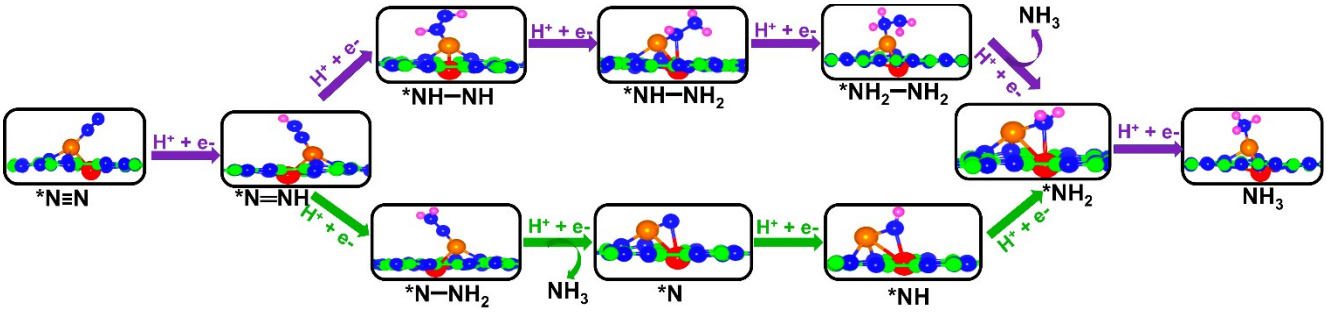

(a)

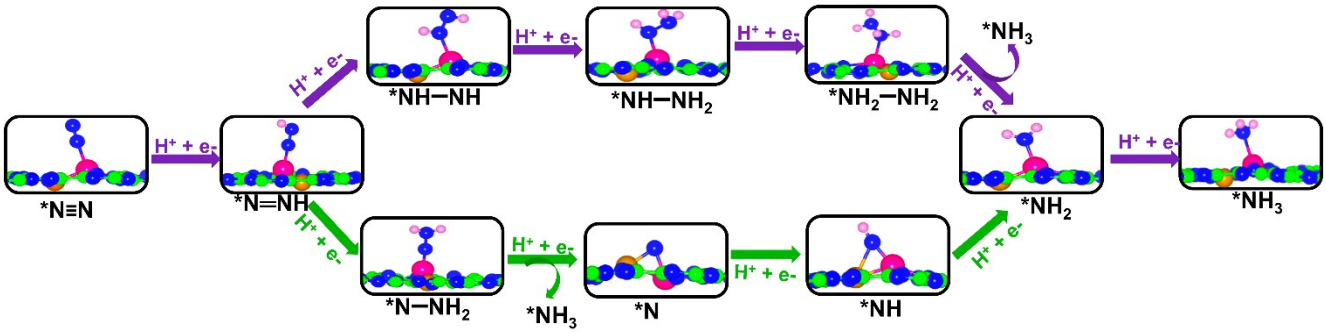

(b)

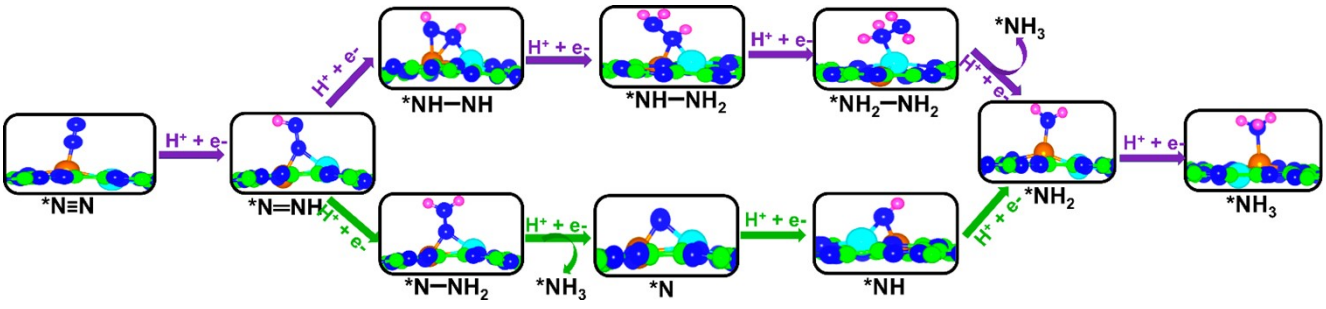

(c)

Fig. S13. Optimized truncated side views of NRR into ammonia intermediates on (a) Fe-La, (b) Fe-Ta and (c) Fe-Ir HDACs along alternating and distal mechanisms. Purple and green coloured arrows indicate alternating and distal mechanisms respectively

Table S3. Comparison of computed limiting potential of present studied best NRR into ammonia catalysts with the already studied systems

Catalyst	**U_L (NH_3) V**
Fe-V and Fe-Ir (Present catalysts)	-0.13 and -0.25 V
Fe-Nb_2C[1]	-0.47 V
MoTi-CG & TiV-CG[2]	-0.34 and -0.30 V
B@GDY, B_2@GDY & B_3@CDY[3]	-0.41, -3.29 and -0.58 V
N_3-Co-Ni-N_2[4]	-0.49 V
Mn_2ON_5/G^{α}[5]	-0.27 V

O-CuCo-N[6]	-0.55 V
$Mn_2@C_3N$ and $Fe_2@C_3N$[7]	(-0.33 V and -0.47 V)
MoW-bN-Pc[8]	-0.32 V
$CaBa@MoSe_2$[9]	-0.60 V
$Mo@Ti_2CO_2$-v and $W@Ti_2CO_2$-v[10]	-0.27 and -0.27 V
W_2@BPN and Ru_2@BPN[11]	-0.29 and -0.30 V
Fe/BNNT, Mn/BNNT, and Pd/BNNT[12]	-0.65, -0.61, and -0.91 V,

Table S4. Comparison of computed limiting potential of present studied best Fe-TM HDACs catalysts for NRR into urea formation via C-N coupling with the reported catalysts

Catalyst	**U_L (NH_2CONH_2) V**
Fe-Y and Fe-Ti (Present catalysts)	-0.62 and -0.84 V
$Ti_2@C_4N_3$ and $V_2@C_4N_3$[13]	-0.741 and -0.738 V
Ta_2@g-C_6N_6[14]	− 1.01 V
Defective Cu-Bi[15]	-0.76 V
B_2@g-C_2N, B_2@g-C_3N_4 and B_2@g-C_6N_6[16]	-2.21, -1.09 and -2.46 V
$ReV@C_2N$[17]	-0.69 V
Mo_2B_2, Ti_2B_2, and Cr_2B_2[18]	-0.49, -0.65, and -0.52 V
$PdCu/TiO_2$[19]	-0.64 V
$Co_2@N_6G$ and $ScNi@N_6G$[20]	-0.61 and -0.99 V
CuPc NTs[21]	-1.67 V
Pd_1Cu_1−TiO_2[22]	-0.84 V
$Sb_xBi_{1-x}O_y$[23]	-1.03 V
$B_{12}@C_2N$[24]	-1.01 V

Table S5: Free energy change of PDS on most promising Fe-TM candidates in consideration of the Hubbard U correction

System	U (Fe)	U (TM)	ΔG_{max}(eV)
Fe-Ti	0	0	0.84
	5.3	3	-0.24
	5	4	-0.36
	5.3	4.5	-0.82
	5	4.5	-0.83
	5	3.5	-0.92
Fe-Y	0	0	0.62
	4	0	-0.28
	4	3	-0.30
	5	3	-0.41
	5.3	0	-0.44
	5	2	-0.48
Fe-Ir	0	0	0.25
	5	2	-0.06
	5	0	-0.03
	4	1.5	0.63
	4	0	0.65
Fe-V	0	0	0.13
	4	3	-0.17
	4	4.1	-0.27
	4	4	-0.27
	4.2	4.1	-0.28
	5.3	4.1	0.73
	5.3	4	0.74

	5	3.4	0.77
	5	3	0.65
	5	4	0.89

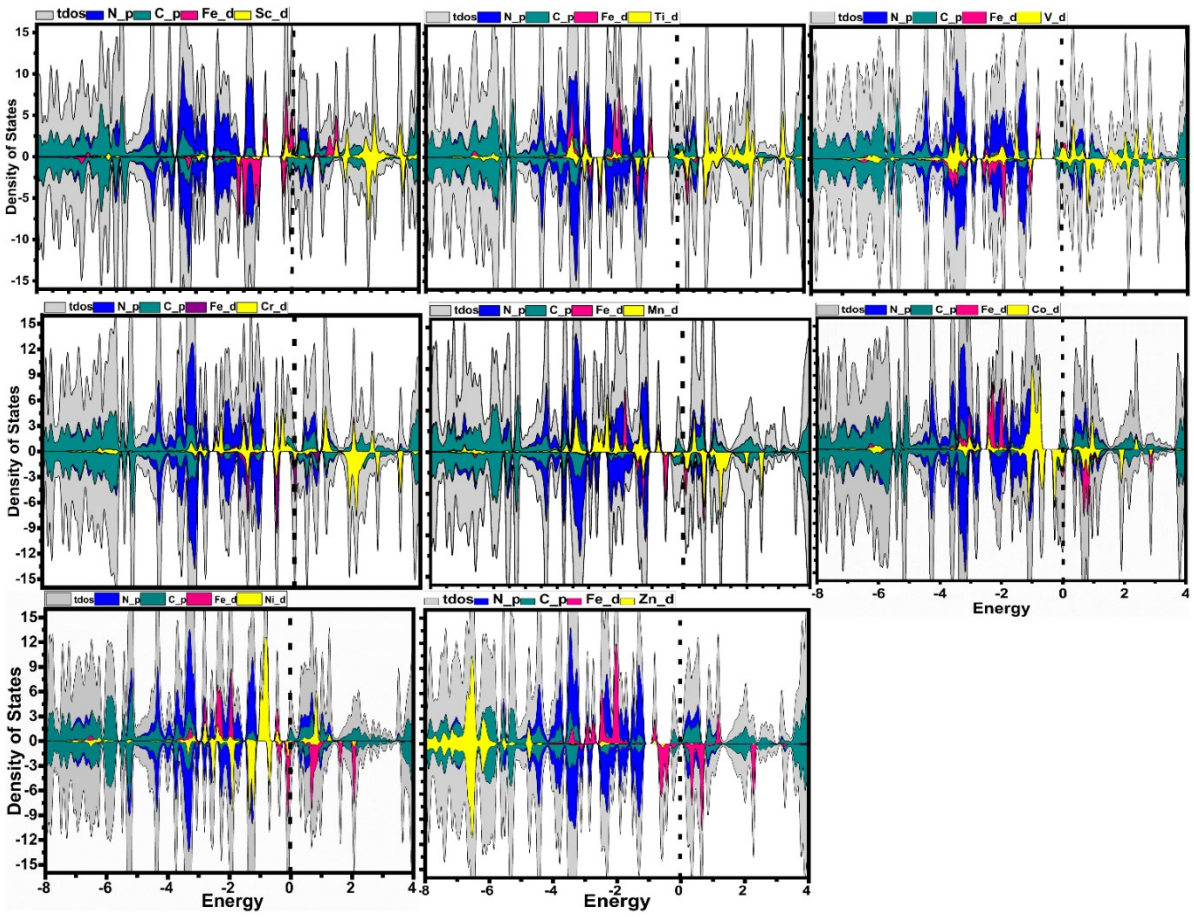

(a)

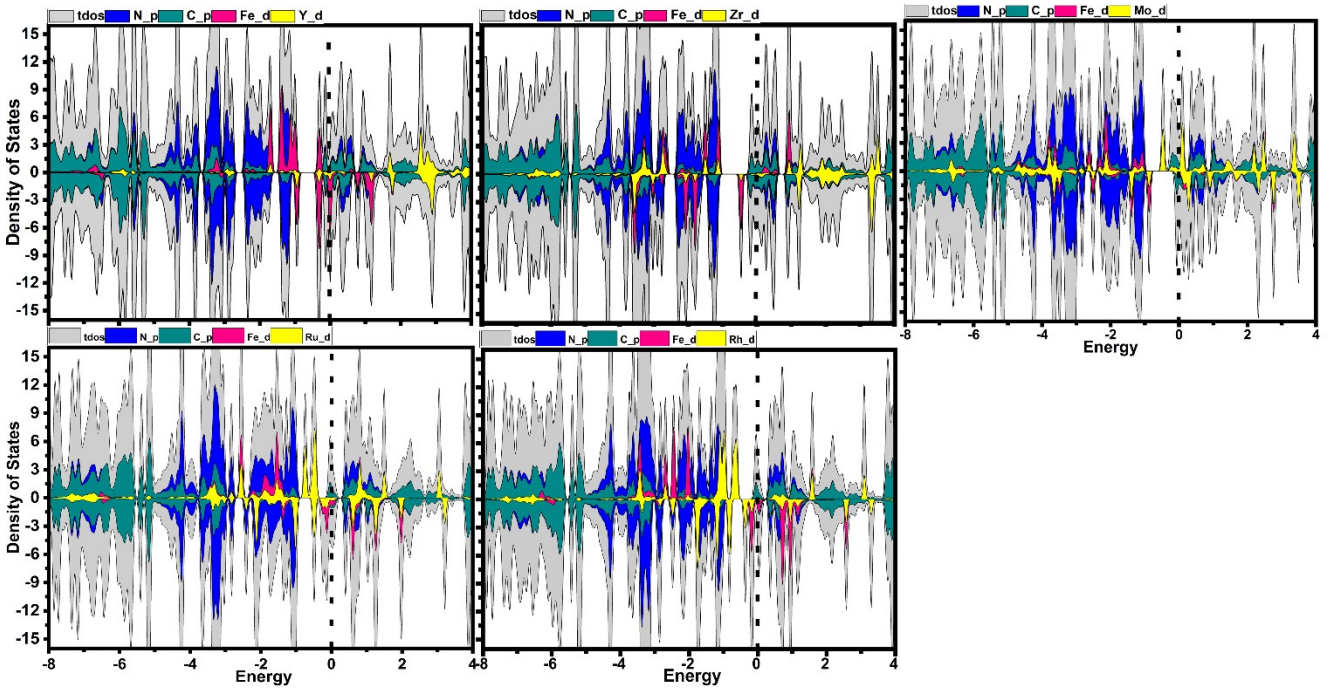

(b)

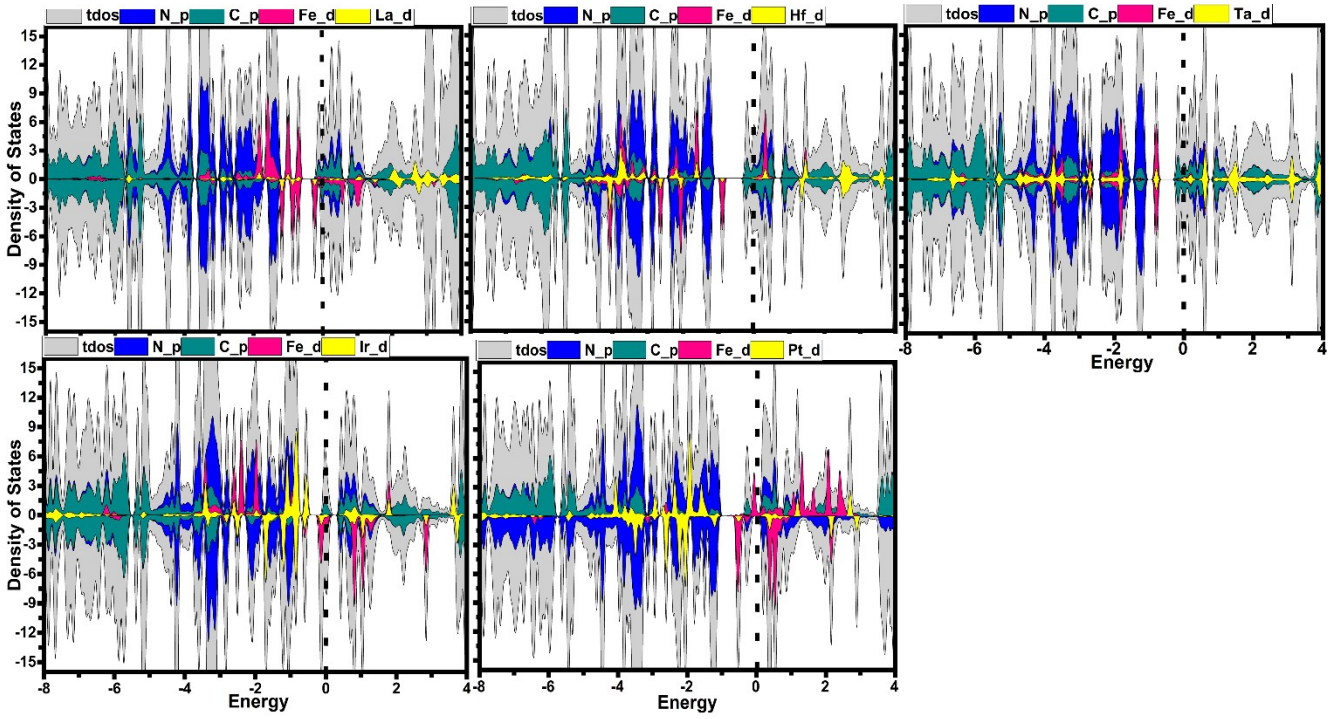

(c)

Fig. S14. The projected density of states (PDOS) of (a) 3d, (b) 4d, and (c)5d transition metal-based Fe-TM HDACs. The PDOS of the total, TM-d, Fe-d, N-2p, and C-2p is plotted in grey, yellow, blue and green colours, respectively.

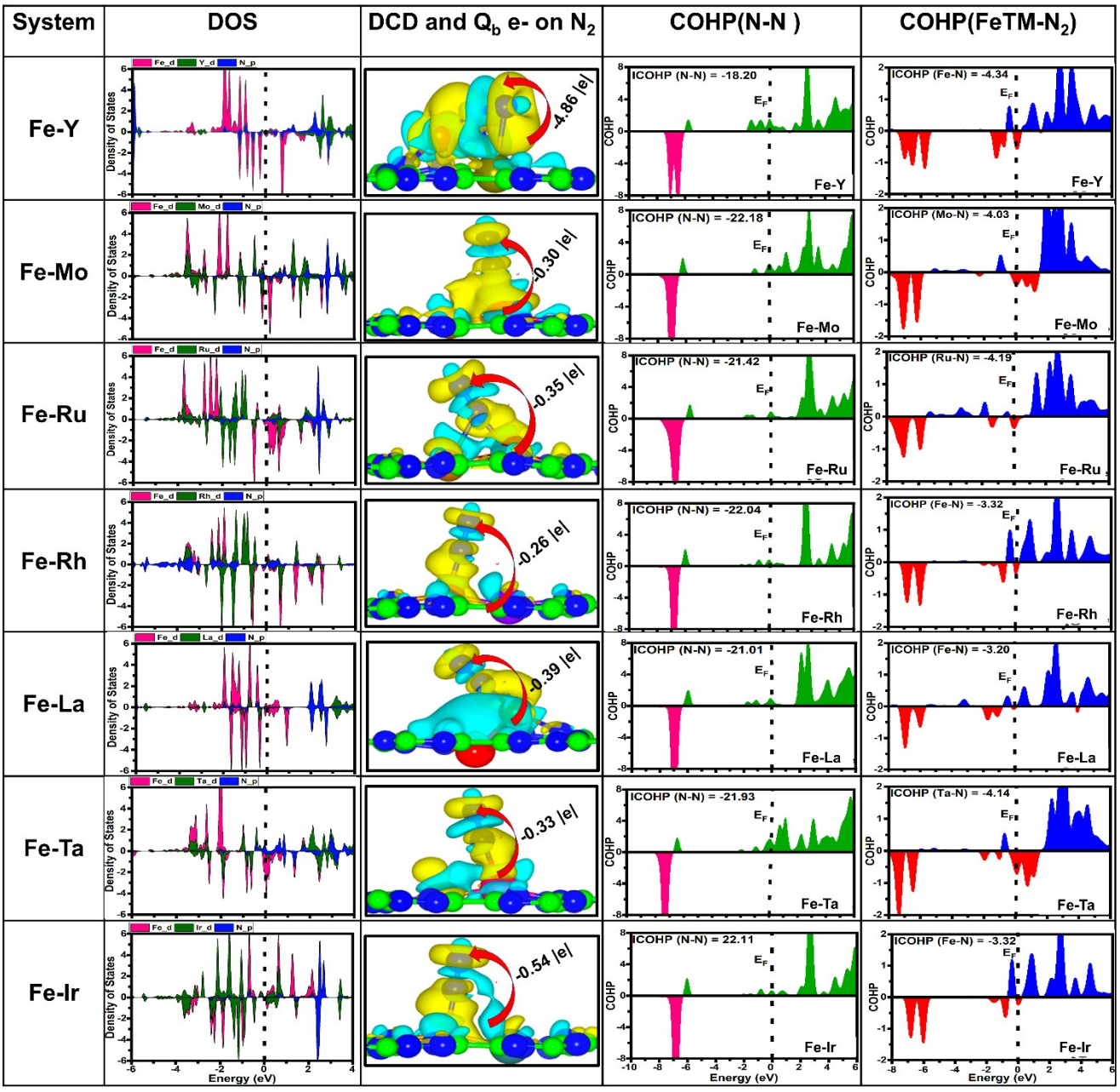

Fig. S15. The projected density of states (PDOS), Charge difference density, and crystal orbital Hamilton population (COHP) of absorbed N_2 on the screened (a) 4d and 5d based Fe-TM systems. The contour level is set to 0.001 e/Å^3. The net Bader charge accumulated on the adsorbed N_2 is depicted using red arrow in the charge density difference plots.

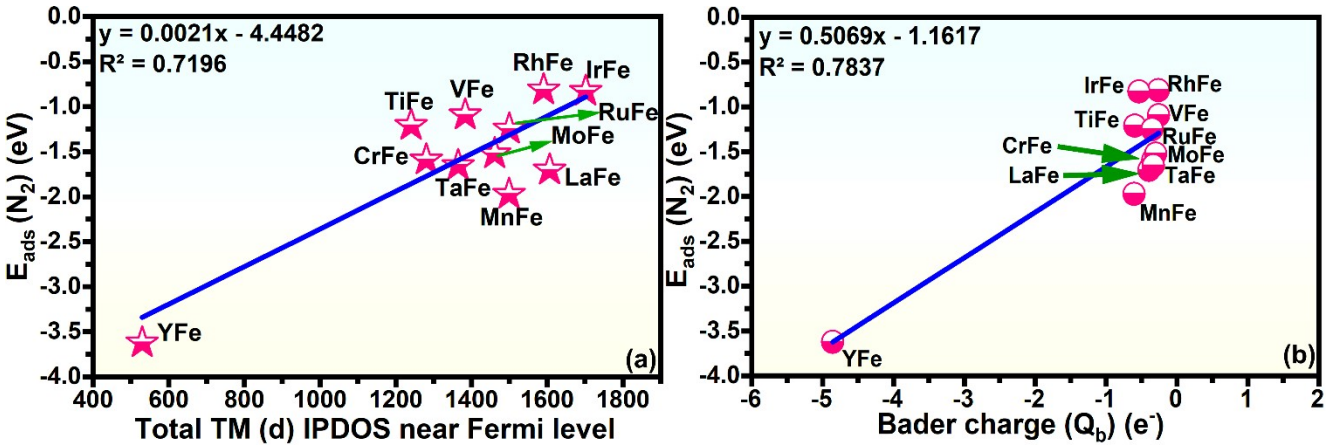

Fig. S16. (a) The relationship between the adsorption energy of the most favorable *N_2 configuration and the Bader charge (Q_b). (b) Linear relation between the adsorption energy of the most favorable *N_2 configuration and total d-states of the transition metal atoms near Fermi level (-1.0 to 1.0 eV).

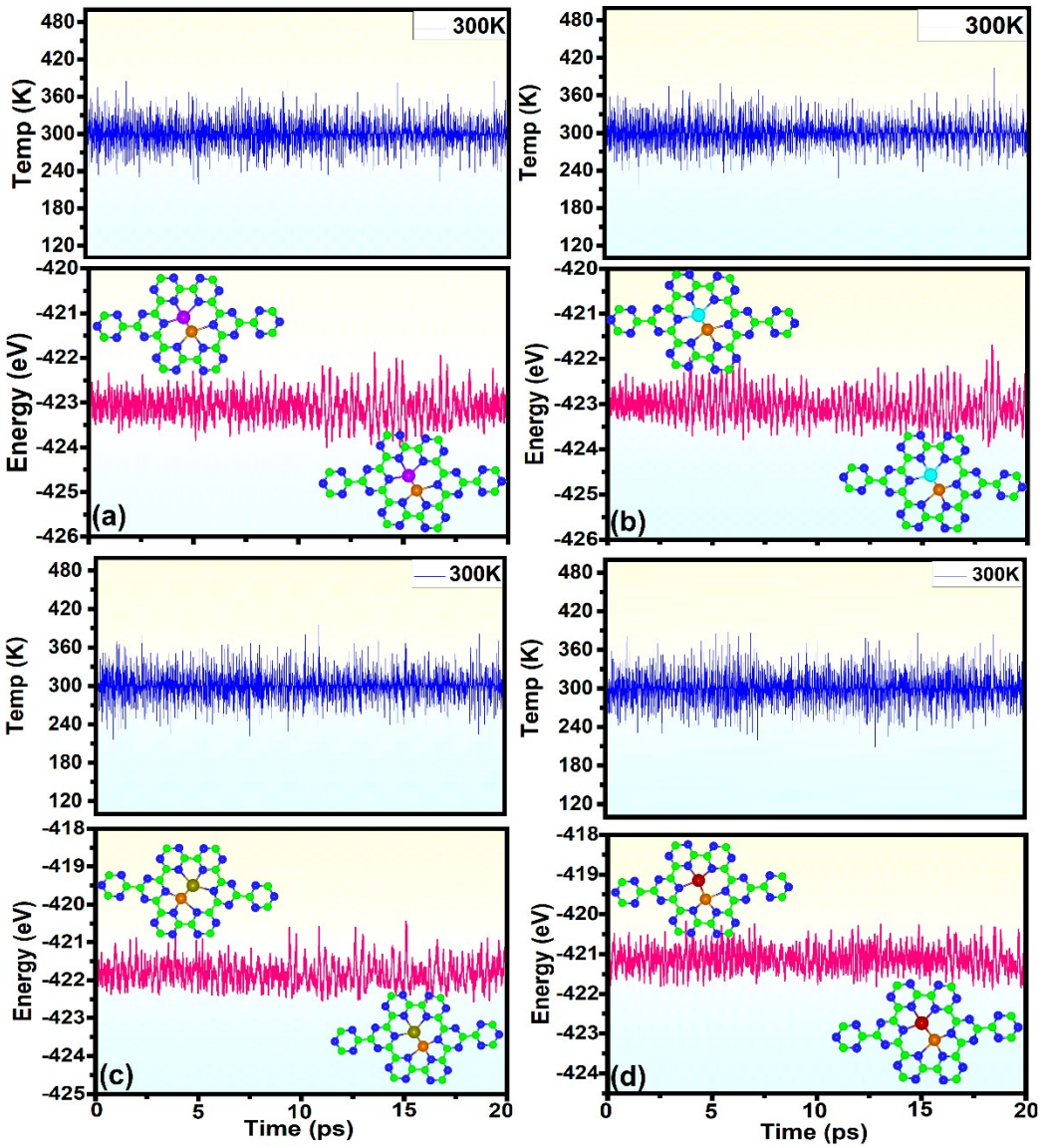

Fig. S17. Fluctuations of temperature and energy during ab-initio Molecular Dynamics (AIMD) simulations of the best catalysts i.e. (a)Fe-V, (b)Fe-Ti, (c)Fe-Y and (d)Fe-Ir at 300 K for 20 ps.

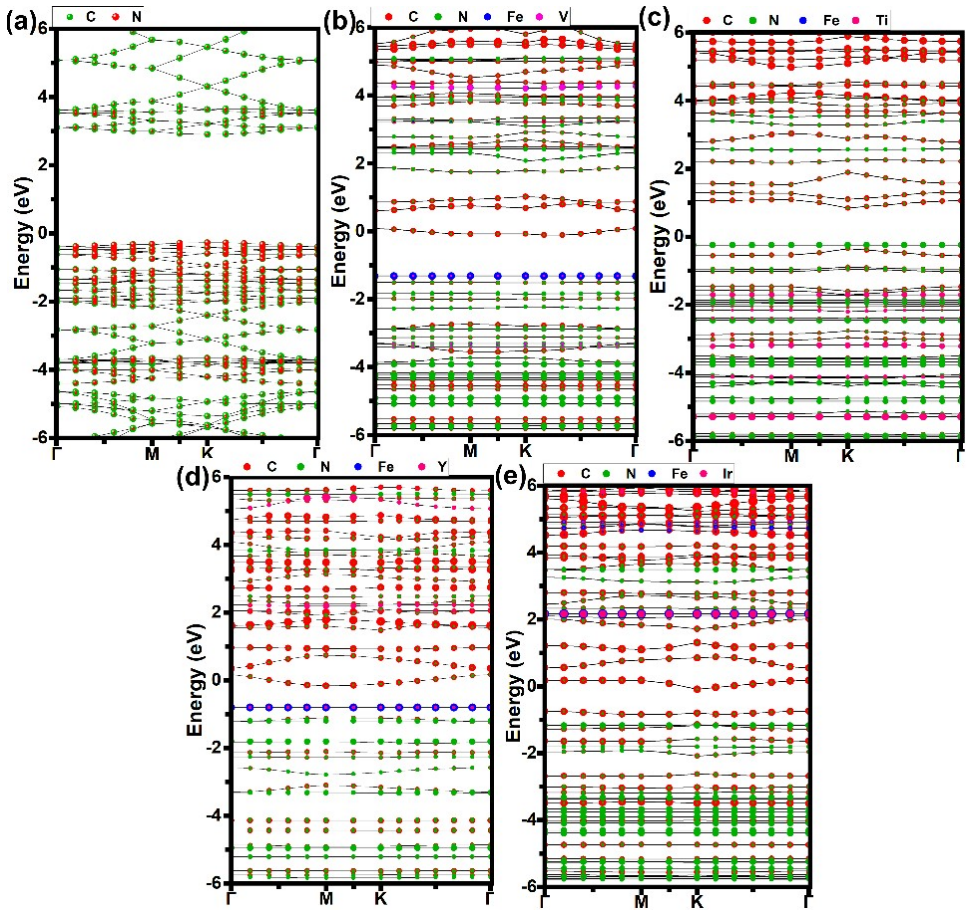

Fig. S18. Electronic band structure of (a) g-C_6N_6 monolayer (b) Fe-V, (c)Fe-Ti, (d)Fe-Y and (e)Fe-Ir.

Table S6. Energy, ZPE, TS, G and ΔG of reaction steps of NRR into urea via direct N_2 and CO_2 coupling on Fe-Ti and Fe-Y along enzymatic and consecutive mechanisms

Enzymatic mechanism on Fe-Ti

System	Energy	ZPE	TS	G	ΔG
$*N_2$	-443.37	0.23	0.12	-443.25	-0.66
$*N_2CO_2H$	-469.60	0.88	0.24	-468.96	0.18
$*N_2CO$	-458.16	0.43	0.20	-457.93	0.22
$*N_2HCO$	-463.27	0.77	0.21	-462.72	-1.32
*NHCO*NH	-467.84	1.10	0.22	-466.96	-2.32
$*NH_2CO*NH$	-471.57	1.45	0.24	-470.36	-2.48
$*NH_2CO*NH_2$	-474.71	1.76	0.28	-473.23	-2.10

Consecutive mechanism on Fe-Ti

System	Energy	ZPE	TS	G	ΔG
$*N_2$	-443.37	0.23	0.12	-443.25	-0.66
$*N_2CO_2H$	-469.60	0.88	0.24	-468.96	0.18
$*N_2CO$	-458.16	0.43	0.20	-457.93	0.22

***N_2HCO**	-463.27	0.77	0.21	-462.72	-1.32
***NH_2CO*N**	-467.292	1.10	0.24	-466.42	-1.79
***NH_2CO*NH**	-471.57	1.45	0.24	-470.36	-2.48
***NH_2CO*NH_2**	-474.71	1.76	0.28	-473.23	-2.10

Enzymatic mechanism on Fe-Y

System	Energy	ZPE	TS	G	ΔG
***N_2**	-443.31	0.20	0.13	-443.24	-3.11
***N_2CO_2H**	-469.73	0.88	0.31	-469.16	-2.49
***N_2CO**	-457.90	0.42	0.16	-457.64	-1.96
***N_2HCO**	-463.62	0.75	0.23	-463.09	-4.16
***NHCO*NH**	-467.79	1.08	0.26	-466.97	-4.80
***NH_2CO*NH**	-471.60	1.42	0.23	-470.41	-4.99
***NH_2CO*NH_2**	-475.29	1.74	0.22	-473.77	-5.11

Consecutive mechanism on Fe-Y

System	Energy	ZPE	TS	G	ΔG
***N_2**	-443.31	0.20	0.13	-443.24	-3.11
***N_2CO_2H**	-469.73	0.88	0.31	-469.16	-2.49
***N_2CO**	-457.90	0.42	0.16	-457.64	-1.96
***N_2HCO**	-463.62	0.75	0.23	-463.09	-4.16
***NH_2CO*N**	-467.82	1.09	0.25	-466.98	-4.81
***NH_2CO*NH**	-471.60	1.42	0.23	-470.41	-4.99
***NH_2CO*NH_2**	-475.29	1.74	0.22	-473.77	-5.11

Table S7. Energy, ZPE, TS, G and ΔG of reaction steps of NRR into ammonia on Fe-V, and Fe-Cr along alternating and distal mechanisms

Alternating mechanism on Fe-V

System	Energy	ZPE	TS	G	ΔG
***N_2**	-443.55	0.20	0.18	-443.53	-0.63
***N_2H**	-447.03	0.51	0.12	-446.64	-0.50
***NHNH**	-450.66	0.83	0.11	-449.94	-0.56
***NHNH**	-454.69	1.161	0.15	-453.68	-1.05
***NH_2NH_2**	-457.54	1.49	0.24	-456.28	-0.41
***NH_2**	-443.15	0.80	0.13	-442.48	-2.59
***NH_3**	-446.97	1.162	0.19	-446.00	-2.87

Distal mechanism on Fe-V

System	Energy	ZPE	TS	G	ΔG
***N_2**	-443.55	0.20	0.18	-443.53	-0.63

***N_2H**	-447.03	0.51	0.12	-446.64	-0.50
***NH_2N**	-450.85	0.83	0.15	-450.16	-0.78
***N**	-434.85	0.09	0.04	-434.80	-1.40
***NH**	-439.19	0.38	0.06	-438.88	-2.23
***NH_2**	-443.15	0.80	0.13	-442.48	-2.59
***NH_3**	-446.97	1.162	0.19	-446.00	-2.87

Alternating mechanism on Fe-Cr

System	Energy	ZPE	TS	G	ΔG
***N_2**	-443.63	0.20	0.17	-443.60	-1.11
***N_2H**	-446.73	0.50	0.14	-446.37	-0.65
***NHNH**	-450.03	0.84	0.14	-449.32	-0.35
***NHNH**	-454.54	1.25	0.08	-453.36	-1.15
***NH_2NH_2**	-457.48	1.60	0.08	-455.96	-0.50
***NH_2**	-443.54	0.86	0.06	-442.72	-3.25
***NH_3**	-446.73	1.16	0.19	-445.75	-3.03

Distal mechanism on Fe-Cr

System	Energy	ZPE	TS	G	ΔG
***N_2**	-443.63	0.20	0.17	-443.60	-1.11
***N_2H**	-446.73	0.50	0.14	-446.37	-0.65
***NH_2N**	-450.53	0.90	0.07	-449.7	-0.73
***N**	-434.66	0.14	0.02	-434.54	-1.55
***NH**	-438.78	0.41	0.04	-438.41	-2.18
***NH_2**	-443.54	0.86	0.06	-442.72	-3.25
***NH_3**	-446.73	1.16	0.19	-445.75	-3.03

Table S8. Energy, ZPE, TS, G and ΔG of reaction steps of NRR into ammonia on Fe-Mn enzymatic and consecutive mechanisms

Enzymatic mechanism on Fe-Mn

System	Energy	ZPE	TS	G	ΔG
***N_2**	-443.01	0.20	0.12	-442.94	-1.46
***N_2H**	-446.30	0.49	0.12	-445.93	-1.21
***NH*NH**	-449.97	0.84	0.11	-449.24	-1.27
***NH*NH**	-453.90	1.19	0.12	-452.83	-1.62
***$NH_{2*}NH_2$**	-458.56	1.40	0.17	-457.33	-2.87
***NH_2**	-442.98	0.86	0.09	-442.21	-3.74
***NH_3**	-445.92	1.16	0.21	-444.98	-3.26

Consecutive mechanism on Fe-Mn

System	Energy	ZPE	TS	G	ΔG
$*N_2$	-443.01	0.20	0.12	-442.94	-1.46
$*N_2H$	-446.30	0.49	0.12	-445.93	-1.21
$*NH_2*N$	-449.78	0.84	0.12	-449.052	-1.09
*N	-434.17	0.14	0.02	-434.052	-2.07
*NH	-438.26	0.43	0.03	-437.86	-2.63
$*NH_2$	-442.98	0.86	0.09	-442.21	-3.74
$*NH_3$	-445.92	1.16	0.21	-444.98	-3.26

Table S9. Energy, ZPE, TS, G and ΔG of reaction steps of NRR into ammonia on Fe-Mo, Fe-Ru and Fe-Rh along alternating and distal mechanisms

Alternating mechanism on Fe-Mo

System	Energy	ZPE	TS	G	ΔG
$*N_2$	-444.51	0.20	0.11	-444.42	-0.92
$*N_2H$	-447.59	0.51	0.13	-447.21	-0.46
*NHNH	-450.97	0.82	0.18	-450.33	-0.34
*NHNH	-455.27	1.16	0.16	-454.27	-1.04
$*NH_2NH_2$	-458.68	1.49	0.23	-457.42	-0.95
$*NH_2$	-443.98	0.92	0.14	-443.20	-2.71
$*NH_3$	-447.81	1.17	0.18	-446.82	-3.09

Distal mechanism on Fe-Mo

System	Energy	ZPE	TS	G	ΔG
$*N_2$	-444.51	0.20	0.11	-444.42	-0.92
$*N_2H$	-447.59	0.51	0.13	-447.21	-0.46
$*NH_2N$	-451.47	0.81	0.19	-450.844	-0.86
*N	-435.45	0.09	0.04	-435.41	-1.400
*NH	-439.95	0.36	0.09	-439.68	-2.43
$*NH_2$	-443.98	0.92	0.14	-443.20	-2.71
$*NH_3$	-447.81	1.17	0.18	-446.82	-3.09

Alternating mechanism on Fe-Ru

System	Energy	ZPE	TS	G	ΔG
$*N_2$	-442.46	0.21	0.155	-442.40	-0.76
$*N_2H$	-445.58	0.52	0.12	-445.18	-0.29
*NHNH	-448.81	0.84	0.14	-448.12	0.02
*NHNH	-453.17	1.15	0.16	-452.17	-0.79
$*NH_2NH_2$	-456.27	1.49	0.22	-455.00	-0.38
$*NH_2$	-442.18	0.86	0.08	-441.40	-2.76
$*NH_3$	-445.37	1.17	0.18	-444.38	-2.49

Distal mechanism on Fe-Ru

System	Energy	ZPE	TS	G	ΔG
$*N_2$	-442.46	0.21	0.155	-442.40	-0.76
$*N_2H$	-445.58	0.52	0.12	-445.18	-0.29
$*NH_2N$	-449.12	0.83	0.15	-448.45	-0.31
*N	-433.12	0.09	0.04	-433.07	-0.91
*NH	-437.23	0.37	0.06	-436.92	-1.53
$*NH_2$	-442.18	0.86	0.08	-441.40	-2.76
$*NH_3$	-445.37	1.17	0.18	-444.38	-2.49

Alternating mechanism on Fe-Rh

System	Energy	ZPE	TS	G	ΔG
$*N_2$	-440.73	0.20	0.18	-440.71	-0.35
$*N_2H$	-444.07	0.52	0.11	-443.65	-0.05
*NHNH	-447.22	0.85	0.13	-446.50	0.34
*NHNH	-451.57	1.16	0.14	-450.54	-0.46
$*NH_2NH_2$	-454.45	1.48	0.17	-453.13	0.20
$*NH_2$	-439.54	0.78	0.16	-438.92	-1.57
$*NH_3$	-443.97	1.15	0.14	-442.96	-2.36

Distal mechanism on Fe-Rh

System	Energy	ZPE	TS	G	ΔG
$*N_2$	-440.73	0.20	0.18	-440.71	-0.35
$*N_2H$	-444.07	0.52	0.11	-443.65	-0.05
$*NH_2N$	-447.50	0.84	0.14	-446.80	0.04
*N	-431.49	0.09	0.04	-431.43	-0.57
*NH	-435.68	0.38	0.05	-435.35	-1.24
$*NH_2$	-439.54	0.78	0.16	-438.92	-1.57
$*NH_3$	-443.97	1.15	0.14	-442.96	-2.36

Table S10. Energy, ZPE, TS, G and ΔG of reaction steps of NRR into ammonia on Fe-La, Fe-Ta and Fe-Ir along alternating and distal mechanisms

Alternating NRR mechanism on Fe-La

System	Energy	ZPE	TS	G	ΔG
$*N_2$	-442.94	0.22	0.16	-442.88	-1.20
$*N_2H$	-446.02	0.50	0.10	-445.62	-0.70
*NHNH	-449.03	0.81	0.14	-448.36	-0.19
*NHNH	-453.43	1.13	0.14	-452.43	-1.03
$*NH_2NH_2$	-456.79	1.50	0.16	-455.44	-0.79

$*NH_2$	-442.55	0.82	0.12	-441.85	-3.18
$*NH_3$	-445.85	1.17	0.17	-444.85	-2.94

Distal mechanism on Fe-La

System	Energy	ZPE	TS	G	ΔG
$*N_2$	-442.94	0.22	0.16	-442.88	-1.20
$*N_2H$	-446.02	0.50	0.10	-445.62	-0.70
$*NH_2N$	-449.44	0.80	0.20	-448.83	-0.67
*N	-433.24	0.08	0.01	-433.17	-0.99
*NH	-438.19	0.35	0.07	-437.91	-2.48
$*NH_2$	-442.55	0.82	0.12	-441.85	-3.18
$*NH_3$	-445.85	1.17	0.17	-444.85	-2.94

Alternating mechanism on Fe-Ta

System	Energy	ZPE	TS	G	ΔG
$*N_2$	-446.34	0.19	0.12	-446.26	-1.14
$*N_2H$	-449.36	0.47	0.18	-449.08	-0.71
*NHNH	-452.79	0.80	0.14	-452.13	-0.51
*NHNH	-457.45	1.13	0.22	-456.55	-1.69
$*NH_2NH_2$	-460.62	1.48	0.19	-459.33	-1.24
$*NH_2$	-446.47	0.81	0.14	-445.81	-3.69
$*NH_3$	-449.78	1.16	0.14	-448.77	-3.41

Distal mechanism on Fe-Ta

System	Energy	ZPE	TS	G	ΔG
$*N_2$	-446.34	0.19	0.12	-446.26	-1.14
$*N_2H$	-449.36	0.47	0.18	-449.08	-0.71
$*NH_2N$	-453.47	0.80	0.20	-452.87	-1.26
*N	-437.61	0.09	0.04	-437.56	-1.93
*NH	-442.18	0.37	0.08	-441.89	-3.02
$*NH_2$	-446.47	0.81	0.14	-445.81	-3.69
$*NH_3$	-449.78	1.16	0.14	-448.77	-3.41

Alternating mechanism on Fe-Ir

System	Energy	ZPE	TS	G	ΔG
$*N_2$	-442.09	0.20	0.17	-442.06	-0.35
$*N_2H$	-445.47	0.53	0.11	-445.05	-0.10
*NHNH	-448.84	0.85	0.10	-448.08	0.10
*NHNH	-453.03	1.164	0.14	-452.01	-0.58
$*NH_2NH_2$	-455.81	1.50	0.15	-454.46	0.22
$*NH_2$	-440.87	0.79	0.15	-440.24	-1.55

***NH_3**	-445.33	1.16	0.13	-444.31	-2.37

Distal NRR mechanism on Fe-Ir

System	Energy	ZPE	TS	G	ΔG
***N_2**	-442.09	0.20	0.17	-442.06	-0.35
***N_2H**	-445.47	0.53	0.11	-445.05	-0.10
***NH_2N**	-449.10	0.85	0.14	-448.40	-0.21
***N**	-433.02	0.10	0.03	-432.96	-0.75
***NH**	-437.18	0.38	0.05	-436.84	-1.40
***NH_2**	-440.87	0.79	0.15	-440.24	-1.55
***NH_3**	-445.33	1.16	0.13	-444.31	-2.37

Reference

1. X. Zhang, L. Yan and Z. Su, *Nanoscale*, 2023, **15**, 17508-17515.
2. R. Hu, Y. Li, Q. Zeng, F. Wang and J. Shang, *ChemSusChem*, 2020, **13**, 3636-3644.
3. I. Anis, S. Amin, G. M. Rather and M. A. Dar, *ChemistrySelect*, 2023, **8**, e202300993.
4. Y. Zhang, Z. Yu, F. She, L. Wei, Z. Zeng and H. Li, *J. Colloid Interface Sci.*, 2023, **640**, 983-989.
5. J. Wu, D. Wu, H. Li, Y. Song, W. Lv, X. Yu and D. Ma, *Nanoscale*, 2023, **15**, 16056-16067.
6. M. Han, Y. Zhang and C. Zhang, *RSC Adv.*, 2024, **14**, 34893-34903.
7. R. Cao, J. Xia and Q. Wu, *Int. J. Hydrogen Energy*, 2024, **54**, 1047-1055.
8. A. Kuma, R. K. Gupta, N. Senthilkumar, B. Pandit, A. M. Al-Enizi and M. Ubaidullah, *Electrocatalysis*, 2024, **15**, 87-95.
9. D. Wu, J. Wu, H. Li, W. Lv, Y. Song, D. Ma and Y. Jia, *J. Mater. Chem. A*, 2024, **12**, 4278-4289.
10. Y. Zhang, N. Ma, Y. Wang, B. Liang and J. Fan, *Appl. Surf. Sci.* , 2023, **623**, 156827.
11. K. Pandiyan, D. K. Dhanthala Chittibabu and H.-T. Chen, *ACS Appl. Energy Mater.*, 2024, **7**, 10758-10769.
12. Y. Liu, H. Zhang and X. Cheng, *Energy Fuels*, 2023, **37**, 13271-13281.
13. J. Liu, X. Lv, Y. Ma, S. C. Smith, Y. Gu and L. Kou, *ACS Nano*, 2023, **17**, 25667-25678.
14. J. Du, H. Wang, C. Yue, I. A. Soomro, M. Pu and M. Lei, *Appl. Surf. Sci.*, 2024, **658**, 159854.
15. W. Wu, Y. Yang, Y. Wang, T. Lu, Q. Dong, J. Zhao, J. Niu, Q. Liu, Z. Hao and S. Song, *Chem Catalysis*, 2022, **2**, 3225-3238.
16. M. A. Dar, *Inorg. Chem*. 2023, **62**, 13672-13679.
17. C. Liu, F. Gong, Q. Zhou and Y. Xie, *Energy Fuels*, 2024, **38**, 8951-8959.
18. X. Zhu, X. Zhou, Y. Jing and Y. Li, *Nat. Commun.*, 2021, **12**, 4080.

19. C. Chen, X. Zhu, X. Wen, Y. Zhou, L. Zhou, H. Li, L. Tao, Q. Li, S. Du and T. Liu, *Nat. chem.*, 2020, **12**, 717-724.
20. C. Zhu, M. Wang, C. Wen, M. Zhang, Y. Geng, G. Zhu and Z. Su, *Adv. Sci.*, 2022, **9**, 2105697.
21. J. Mukherjee, S. Paul, A. Adalder, S. Kapse, R. Thapa, S. Mandal, B. Ghorai, S. Sarkar and U. K. Ghorai, *Adv. Funct. Mater.*, 2022, **32**, 2200882.
22. L. Pan, J. Wang, F. Lu, Q. Liu, Y. Gao, Y. Wang, J. Jiang, C. Sun, J. Wang and X. Wang, *Angew. Chem.*, 2023, **135**, e202216835.
23. X. Chen, S. Lv, J. Kang, Z. Wang, T. Guo, Y. Wang, G. Teobaldi, L.-M. Liu and L. Guo, *Proc. Natl. Acad. Sci.*, 2023, **120**, e2306841120.
24. Y. Cao, Y. Meng, R. An, X. Zou, H. Huang, W. Zhong, Z. Shen, Q. Xia, X. Li and Y. Wang, *J. Colloid Interface Sci.*, 2023, **641**, 990-999.